Accuracy of native myocardial T1 and T2 mapping for quantifying ischemic myocardial scar

Leila Haririsanati (MSc. Candidate)
Experimental Medicine, McGill University, Montreal
June 2022

A thesis submitted to McGill University in fulfilment of the requirement of the degree of Master in experimental medicine (REB#2021-7566)

Accuracy of native myocardial T1 and T2 mapping for quantifying ischemic myocardial scar

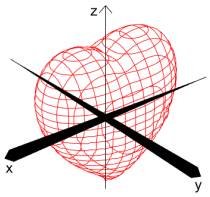

Tissue Team

Leila Haririsanati (MSc. Candidate)
Experimental Medicine, McGill University, Montreal
June 2022

A thesis submitted to McGill University in fulfilment of the requirement of the degree of Master in experimental medicine (REB#2021-7566).

ABSTRACT

Background: Cardiac magnetic resonance imaging (CMR) with late gadolinium enhancement (LGE) is the clinical gold standard method to assess irreversible injury and fibrosis visually and quantitatively in patients with ischemic cardiomyopathy (ICMP). LGE however is time-consuming, costly, and may have side effects. Native (contrast-free) T1 and T2 mapping are altered by these tissue pathologies and therefore have the potential to replace contrast-enhanced LGE imaging. We evaluated the accuracy of native T1 and T2 mapping to detect the presence, location, and size of irreversible myocardial injury, using LGE as a standard of truth, in patients with ICMP.

Methods: We retrospectively studied patients with suspected ICMP who had undergone a clinical exam including LGE, T1 maps and T2 maps. In a blinded analysis, the irreversible injury was defined in LGE images as an area with increased signal intensity (> 5 standard deviations (SD) above reference tissue). In the T1 and T2 maps, this pathologic area was defined as an increase of ≥ 2 SD above our local normal reference values. The presence and extent of the areas identified as abnormal were compared between paired short-axis T1 maps and LGE images. The acute injury was identified based on elevated T2 times.

Results: We enrolled 32 patients (mean age 64±13 years old, 9% females). There was a moderate to a strong agreement between T1 maps and LGE (Kappa for basal 0.87, mid-ventricle 0.93, apex 0.66) in identifying the presence of myocardial injury. The agreement between T2 maps and LGE in all slices was moderate to strong (Kappa for basal 0.65, mid-ventricular 0.82, apex 0.68). The extent of myocardial injury in chronic cases was not significantly different between LGE and T1 maps ($p=0.31$). In slices with the presence of acute injury, 57% of total slices, T1 maps identified a significantly larger area of myocardial injury than LGE ($p<0.001$). However, T2 maps and LGE had a similar extent of myocardial injury (with p values: apex= 0.45, mid-ventricle= 0.18, basal= 0.18).

Conclusions: In patients with acute or chronic ischemic myocardial injury, there is a moderate (apex) to strong (mid and basal) agreement between T1 maps, T2 maps and LGE in identifying the area of ischemic myocardial injury. In slices with chronic injury, the extent of the injured area was similar between T1 maps and LGE. In slices with evidence of acute injury, the extent of myocardial injury was similar between T2 maps and LGE. These findings suggest that non-contrast images may be useful in identifying the location and extent of myocardial injury. While T1 allows for estimating the size of chronic injury, T2 does so for acute injury. Future studies in larger samples should be performed to investigate the utility of combining image information from both T1 and T2 maps.

RESUME

Contexte : L'imagerie par résonance magnétique cardiaque (IRM) avec rehaussement tardif au gadolinium (LGE) est la méthode clinique de référence pour évaluer visuellement et quantitativement les lésions irréversibles et la fibrose chez les patients atteints de cardiomyopathie ischémique (ICMP). Cependant, LGE prend du temps, coûte cher et peut avoir des effets secondaires. La cartographie native (sans contraste) T1 et T2 est altérée par ces pathologies tissulaires et a donc le potentiel de remplacer l'imagerie LGE à contraste amélioré. Nous avons évalué la précision de la cartographie native T1 et T2 pour détecter la présence, l'emplacement et la taille d'une lésion myocardique irréversible, en utilisant le LGE comme norme de vérité, chez les patients atteints d'ICMP.

Méthodes : Nous avons étudié rétrospectivement des patients suspectés d'ICMP qui avaient subi un examen clinique incluant LGE, cartes T1 et cartes T2. Dans une analyse en aveugle, une lésion irréversible a été définie dans les images LGE comme une zone avec une intensité de signal accrue (> 5 écarts-types (SD) au-dessus du tissu de référence). Dans les cartes T1 et T2, cette zone pathologique a été définie comme une augmentation de ≥ 2 SD au-dessus de nos valeurs de référence normales locales. La présence et l'étendue des zones identifiées comme anormales ont été comparées entre les cartes T1 appariées à petit axe et les images LGE. Une blessure aiguë a été identifiée sur la base des temps T2 élevés.

Résultats : Nous avons recruté 32 patients (âge moyen 64 ± 13 ans, 9 % de femmes). Il y avait un accord modéré à fort entre les cartes T1 et LGE (Kappa pour basal 0,87, mi-ventricule 0,93, apex 0,66) pour identifier la présence d'une lésion myocardique. L'accord entre les cartes T2 et LGE dans toutes les tranches était modéré à fort (Kappa pour basal 0,65, mi-ventriculaire 0,82, apex 0,68). L'étendue de la lésion myocardique dans les cas chroniques n'était pas significativement différente entre les cartes LGE et T1 (p = 0,31). Dans les tranches avec présence de lésions aiguës, 57 % des tranches totales, les cartes T1 ont identifié une zone significativement plus grande de lésions myocardiques que LGE (p <0,001). Cependant, les cartes T2 et LGE avaient une étendue similaire de lésion myocardique (avec des valeurs p : apex = 0,45, ventricule moyen = 0,18, basal = 0,18).

Conclusions : Chez les patients présentant une lésion myocardique ischémique aiguë ou chronique, il existe une concordance modérée (apex) à forte (moyenne et basale) entre les cartes T1, T2 et LGE pour identifier la zone de lésion myocardique ischémique. Dans les tranches avec blessure chronique, l'étendue de la zone lésée était similaire entre les cartes T1 et LGE. Dans les tranches présentant des signes de lésion aiguë, l'étendue de la lésion myocardique était similaire entre les cartes T2 et LGE. Ces résultats suggèrent que des images sans contraste peuvent être utiles pour identifier l'emplacement et l'étendue de la lésion myocardique. Alors que T1 permet d'estimer la taille des blessures chroniques, T2 le fait pour les blessures aiguës. Des études futures sur des échantillons plus importants devraient être réalisées pour étudier l'utilité de combiner les informations d'image des cartes T1 et T2.

ACKNOWLEDGEMENT

This master thesis couldn't have been possible without the contribution of many people. I am grateful to all of those with whom I had the pleasure to work.

First, I would like to thank my supervisor, Dr. Matthias G. Friedrich, who gave me the opportunity to conduct this master thesis and provided me with professional mentorship and taught me a great deal about how to conduct scientific research.

I would like to also thank Dr. Shafat Rabbani, Dr. Abhinav Sharma, and Dr. Josephine Pressacco from my master's committee, who have provided guidance throughout this educational journey. I am especially grateful to Dr. Elizabeth Hillier for her mentorship and countless time to answer any of my questions, guide me through the scientific process, and teach me CMR analysis.

I would like to thank Katerina Eyre, Ph.D. candidate for her endless support and many hours in guiding me in conducting research, CMR physics, statistics, interpreting the results, and writing my thesis. Her supportive nature made for a pleasant work environment, where I felt comfortable and enjoyed working with.

Furthermore, I would like to thank Dr. Michael Chetrit for his clinical comments during this thesis and supports with his knowledge in cardiology and CMR imaging, and Dr. Ria Garg, who was always available for advice throughout my master's and supports the clinical aspect of this thesis.

Thank you to both, Adonis Rodaros and Elizavet Konidis, for being great research coordinators who help me to conduct my research.

I would like to acknowledge the remaining member of the CMR research lab and Tissue team: Dr. Mitchel Benovoy, Dr. Andrew Coristine, and Saad Razzaq for their feedback and encouragement during our many team meetings. There were many people who contributed to my work as well. Special thanks to both Sylvie Gelineau and Margherita Leo for their effort in the CMR image acquisition that I used for completing my master thesis. Last, but not least, I would like to thank Kathleen Amedee, Julie Lebel, Jeannette Piedade, Filipe Henriques, Florianne Amedee, and Fatima Hafdi for their help in the administrative aspects of the thesis.

I would like to acknowledge the support of my family. To my sibling, Saeed, thank you for all the encouragement during my master's years. A special thank-you to my dearest parents for providing me with endless emotional support throughout my entire master's program and celebrating each step along this journey.

To my dearest husband, Houman, thank you for all your patience and support in completing this master's. Finally, to my precious daughters, Parmis and Pania, for motivating me in every

challenge that I faced to put all my effort into and for being enough patient on this journey with me. I hope this master inspired them to have perseverance in life.

LIST OF TABLES

LIST OF FIGURES

List of Abbreviations

CAD: Coronary artery disease
CMR: Cardiac magnetic resonance imaging
SAX: Short axis
2CH: Two chambers
3CH: Three chambers
4CH: Four chambers
TE: Echo time
TR: Repetition time
ICMP: Ischemic cardiomyopathy
LAD: Left anterior descending artery
LAX: Long axis
LCX: Left circumflex
LV: Left ventricle
LGE: Late gadolinium enhancement
MOLLI: Modified look locker inversion recovery
RCA: Right coronary artery
RF: Radiofrequency
ROI: Region of interest
SD: Standard deviation
T: Tesla

Table of Contents

CONTRIBUTION OF AUTHORS:

All the writing in this thesis is the work of the main author, Leila Haririsanati (LH), All the tables and figures were designed and generated by LH (All chapters). The contribution of Dr. Matthias G. Friedrich (MF) with his expertise in cardiology and cardiovascular magnetic resonance imaging (CMR) made this thesis possible (All chapters).

Katerina Eyre (KE) brought her knowledge in statistics, CMR physics, interpreting the results, and writing this thesis (All chapters).

Elizabeth Hillier (EH) contributed to this thesis with her knowledge of CMR innovation and its application (Chapters 3 and 4).

The accuracy and reproducibility of the results were ensured by an additional analysis for late gadolinium enhancement and mapping analysis by Dr. Michael Chetrit (MC) (Chapters 1 and 2) and Dr. Ria Garg (RG) (Chapters 1 and 2). Additionally, their expertise in cardiology guided LH in understanding the clinical aspect of this work.

Thesis Objectives:

Native T1 and T2 mapping may have the potential to be applied in routine clinical imaging for myocardial tissue characterization.

The objective of this study was to assess the agreement between the native mapping and LGE in ischemic cardiomyopathy patients to identify the presence, pattern, and extension of the myocardial injury.

CHAPTER 1

1. INTRODUCTION

1.1. ISCHEMIC CARDIOMYOPATHY

Coronary artery disease, the leading cause of death around the world, is characterized by the formation of intracoronary plaques that eventually may lead to a narrowing or complete blockage of the coronary vessels with subsequent perfusion deficits and resulting ischemic injury (Figure 1) (2)(3)(4). The mismatch between blood supply and demand in the heart leads to the death of cardiomyocytes, an event clinically referred to as myocardial infarction. If survived, such an event may lead to chronic ischemic cardiomyopathy (ICMP) (1), with decreased ventricular function and heart failure.

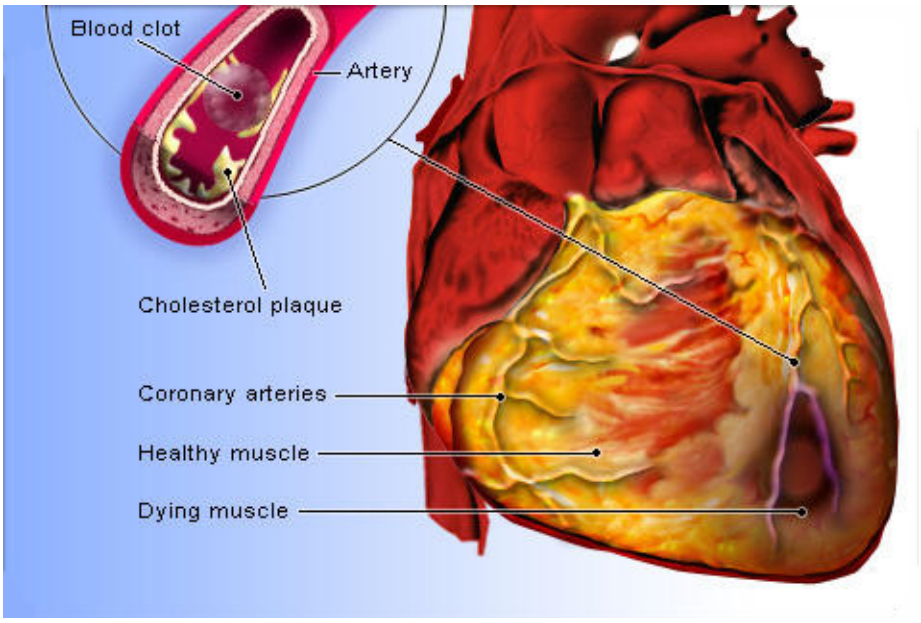

Figure 1: **Myocardial tissue damage**: Myocardial infarction due to coronary artery blockage. The image presents the ischemic tissue damage (darker colour) in the myocardium that is supplied by the blocked artery (1).

The myocardial tissue changes in ischemic cardiomyopathy start with cellular hypoxia that, if persistent, result in the death of myocytes. This insult activates inflammatory cells including white blood cells (neutrophils) that migrate to the infarcted area (day 1 to 3) (11) to remove dead myocytes (12). These are followed by macrophages that clean the tissue from inflammatory debris (day 3 to 7) (11). This process is accompanied by an increase in water content known as edema. Edema is therefore an important factor to discriminate between acute and chronic myocardial insults. To identify the presence of edema in the myocardium, edema imaging such as mapping with cardiac magnetic resonance imaging can be an asset.

Inflammatory cells activate the reparative and proliferative phases, which start from three to eight weeks of injury to support the infarcted heart tissue by re-establishing a myocardial matrix network (13). In this phase, the production of type 1 collagen in the extracellular space increases and leads to the formation of a permanent scar approximately at the end of the second month. Of note, scar tissue does not contain cardiomyocytes and therefore does not contribute to contractile function (11) (14). Scar tissue can be identified by cardiac magnetic resonance imaging, specifically late gadolinium enhancement imaging and, more recently, mapping (46).

The infarct shrinks to 25% of its volume during the acute phase after four to six weeks, mainly because of the resolution of the edema, with fibrotic tissue remaining in the myocardium (16) (17).

1.2. CARDIAC MAGNETIC RESONANCE IMAGING AND ASSESSMENT OF ISCHEMIC MYOCARDIAL TISSUE INJURY

Ischemic myocardial injury can lead to further cardiovascular events including heart failure, which emphasizes the importance of accurate assessment of myocardial injury to improve patient's management and prognosis (5)(6). Coronary angiography, which is a real-time, invasive imaging methodology, can detect the culprit coronary artery and the severity of stenosis. In this method, a catheter is inserted into the body to inject the contrast dye and visualize the occlusion by x-rays. Non-invasive computed tomography (CT) can also be used to perform coronary angiography. In acute clinical settings (coronary occlusion during the recent hours), this can inform revascularization of the blocked artery, limiting the expansion of irreversible injury during the first hours of no-flow ischemia and help preserve LV dysfunction (7)(8). There are some risks associated with coronary angiography, including radiation, bleeding at the catheter insertion site, and side effects associated with the contrast agent. Furthermore, significant costs are associated with such a procedure.

Cardiac magnetic resonance (CMR) is an imaging modality that can evaluate the etiology of myocardial injury and identify the culprit coronary artery (18) (19) with fewer side effects and lower risk. CMR is also considered the gold-standard method for non-invasively characterizing myocardial tissue with a high spatial resolution (9), free choice of imaging planes, and lack of ionizing radiation (10).

CMR allows for assessing tissue changes such as hemorrhage, edema, and fibrosis. It can demonstrate the presence of viability and thereby predict the functional recovery after

revascularization (18)(19), helping therapeutic decision-making, specifically on the indication for revascularization procedures (8).

1.2.1. Introduction to CMR

Magnetic resonance imaging (MRI) uses the exchange of energy between a strong magnetic field (B0) and protons in the tissue. MRI requires a strong magnet with a gradient system to generate high-frequency impulses, coils (acting as antennas), and hardware/software to construct images from primary MR data (20).

1.2.1.1 Image Acquisition

When an individual is placed in the scanner with a static magnetic field (B0), the hydrogen protons in water molecules (Figure 4), an abundant molecule in our body, align toward the direction of the magnetic field of the scanner (B0) (48). These hydrogen protons have a small spin on their axis like a gyroscope, and in the absence of a magnetic field, they spin in randomly distributed directions.

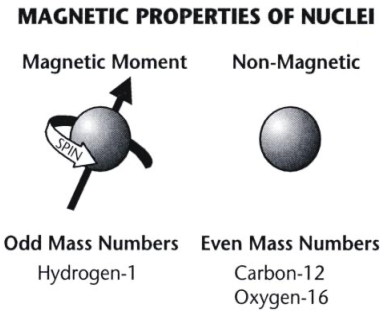

Figure 2: Magnetic and non-magnetic nuclei*:* Nuclei with an odd number of hydrogens create magnetic properties in the static magnetic field of the scanner (2).

In the presence of a magnetic field, spins align in the direction of the magnetic field (21) at a stable frequency called the Larmor frequency. The Larmor frequency is dependent on the magnetic field strength and creates a net magnetization (M0) (21) (22).

The MRI signal is generated by radio frequency (RF) pulses which deliver energy to target protons and excite them from their original, equilibrium to a higher energy state (22) (23). Different sets of RF pulses are utilized in so-called 'sequences' to produce images with specific signal intensity properties that generate contrasts that in turn allow for visualizing various tissues depending on their molecular composition (24).

When the RF source is turned off, the created magnetization in the protons (B1) returns to its resting state (equilibrium), and a signal (radio wave) is emitted. Receiver coils are used, typically on the surface of the body ('surface coils') to detect and capture the emitted signal. This raw MR signal is stored in a mathematical matrix called k-space and is used to reconstruct MRI images (23) (25).

MRI uses three gradient coils to cover each spatial dimension in an image (X, Y, and Z) (22). The gradients vary the magnetic field strength linearly along their respective axis. This results in a slight but predictable disjunction of proton spin alignment. The use of gradients across all three spatial planes allows for the spatial encoding of the MRI data during image reconstruction (**Figure 3**) (26)(27).

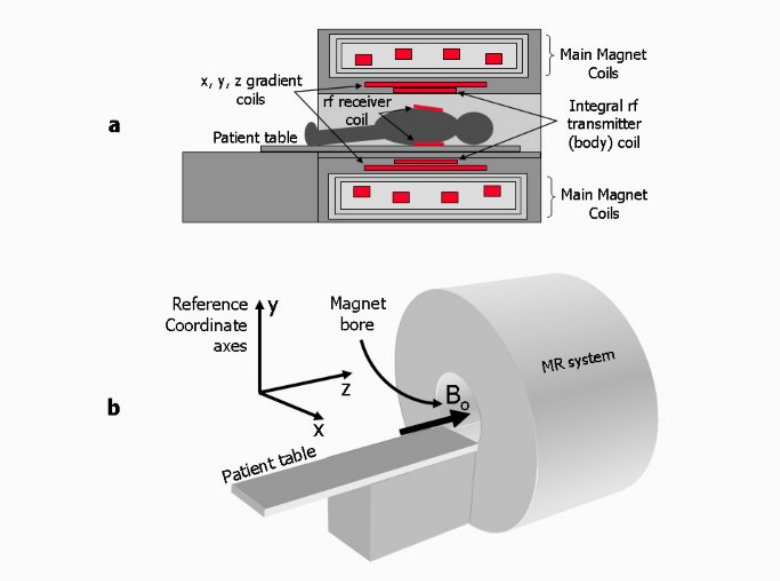

Figure 3: MRI system: The diagram shows the location of the main magnet coils, x, y, and z gradient, RF transmitter body coil and RF receiver coils (3).

1.2.1.2. Relaxation Constants*:*

As soon as RF pulses are removed, protons transition from an excited state of resonance to their equilibrium state occur. This is referred to as relaxation. The environment within which protons are contained determines the speed at which they relax to equilibrium. Thus, relaxation times are specific for each tissue and can be used to identify each tissue separately (25)(28).

Two different types of relaxation are typically considered in MRI: longitudinal relaxation (T1 relaxation) and transverse relaxation (T2 relaxation). T1 relaxation refers to the relaxation rate associated with the release of energy from the spinning molecule to its surrounding environment. It starts rapidly, and when it reaches the equilibrium state, it slows down (22). T2 relaxation refers to the rate of relaxation associated with the release of energy from the spinning molecule to its

neighbouring proton. These two relaxations happen simultaneously and create contrast in MRI images based on the pulse sequence design that emphasizes one of them.

Different tissues have various protons, each is spinning with a specific frequency. The rate of proton's motion, called "precession", is related to the magnetic field strength, which is constant. Still, it is feasible that one proton is spinning with a slightly different frequency from the neighbouring protons because protons are within molecules and are moving rapidly in a random fashion. This causes the proton's spin to move out of phase (de-phasing) and result in spin decay, which is called T2 relaxation. Since T2 relaxation is due to the interaction of neighbouring protons' spin, it is called spin-spin relaxation (29).

Different T1 and T2 relaxation rates in the tissues create different contrast in images which is the base of CMR imaging. These differences are based on their image acquisition parameters, such as the echo time (TE) and repetition time (TR) that create image contrast in T1 and T2 weighted sequences. TE is the time between delivery of the RF and receiving the echo signal. TR is the time between two consecutive pulse sequences on the same slice. T1 weighted images have short TE and TR, while T2 one has long TE and TR (Figure 4). In T1 weighted images, the T1 property of the tissue is responsible for creating the contrast between different structures. For instance, fat presents as white, and water appears dark. In T2 ones, the T2 property creates the contrast; fat appears white, muscle is grey, and fluid is white (29).

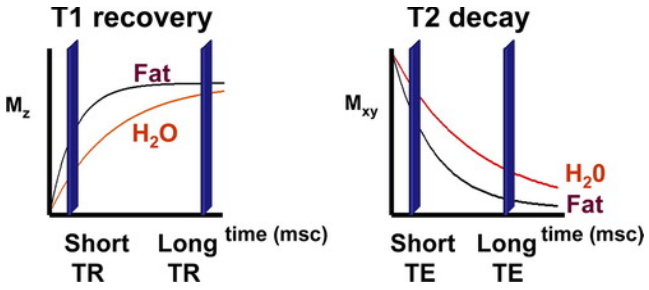

Figure 4*:* The differences between fat and water in the T1 recovery curve with manipulation of the reptation time (TR). The differences in T2 decay of water and fat and manipulation of echo time (TE) contrast in tissues with fat and water content (4).

Besides, manipulation of the magnetic properties of the tissue by their relaxation rate, a contrast medium such as gadolinium can be applied to enhance the contrast between different tissues in MR imaging. Gadolinium causes the T1 relaxation rate to increase and the fibrotic myocardium presented with brighter contrast (30). The application of gadolinium is explained further in this thesis.

1.2.1.3 Late Gadolinium Enhancement CMR (LGE-CMR)

Image acquisition after 10 to 20 minutes of gadolinium administration can detect irreversible cardiac tissue damage (fibrosis). This method is called Late Gadolinium Enhancement (LGE) CMR (31) (32). Late gadolinium enhancement CMR imaging is the gold standard method in scar imaging because of its high sensitivity for detecting focal myocardial fibrosis in tissue damage (31).

Gadolinium is an extracellular agent which cannot enter the cardiac cells with an intact membrane due to its large size. It washes out rapidly from the heart with normal coronary

circulation (32). CMR images with gadolinium usage in the normal myocardium display the same contrast before and after its administration.

1.2.1.3.1 LGE Image Acquisition

In acute myocardial injury, the cell membrane is ruptured and increases the relative proportion of extracellular space. Gadolinium, with its primarily extracellular distribution, will enter this space, from which its washout takes more time than from tissue with an only small proportion of extracellular space (such as healthy tissue). In chronic cases, the extracellular space is expanded by the fibrous structures that also increase the volume of distribution for gadolinium, causing a relative delay in the washout of gadolinium from this space (33). Fig. 5 summarizes these mechanisms. (**Figure 5).**

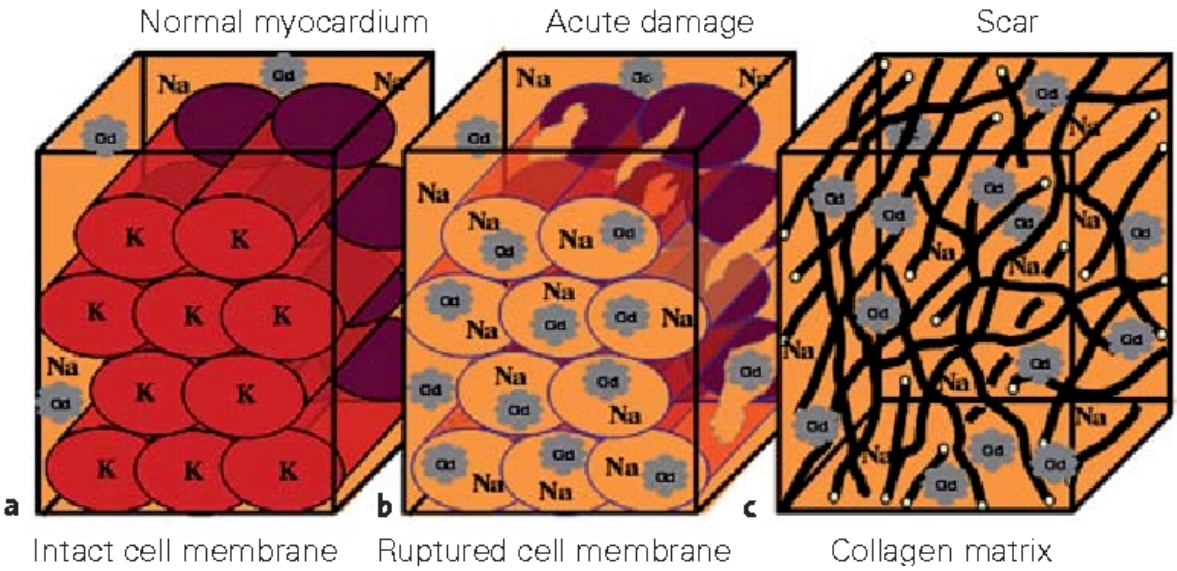

Figure 5: Gadolinium (Gd) distribution's mechanism in acute and chronic myocardial injuries (5)

a: In healthy myocardium, the proportion of extracellular volume is small, associated with a rapid washout of gadolinium

b: In acute myocardial infarction, the cardiomyocyte membranes are ruptured, and Gd is trapped

inside the cells, with a delayed washout.

c: In chronic myocardial infarction, the extracellular space is expanded because of its presence in the extracellular matrix, again leading to a delay of Gd washout.

For minimizing the signal of normal myocardium, LGE imaging uses an inversion time (TI), the waiting time between a preparation pulse of 180-degree (inverting pulse) and 90-degree pulse (34), to artificially 'null' normal myocardium, thereby create a stark contrast between normal and irreversibly injured myocardium.

If performed properly, the scar is visible as an area with high signal intensity within the myocardium. In cases where there is a thin subendocardial layer of dead myocytes, however, the scar may be difficult to discriminate from intracavitary blood. This may limit the visual detectability of subendocardial infarcts (35). One approach to identifying the high-intensity signal of scar from blood is to compare LGE images to CINE images (35), which allows for defining regional wall versus subendocardial scar and blood (35).

The other technique is applying an LGE sequence with dark blood properties (36), where blood appears dark which makes the sub-endocardial scar appears bright and can differentiate a thin subendocardial infarction scar and assess accurately the level of transmurality (36) (Figure 6).

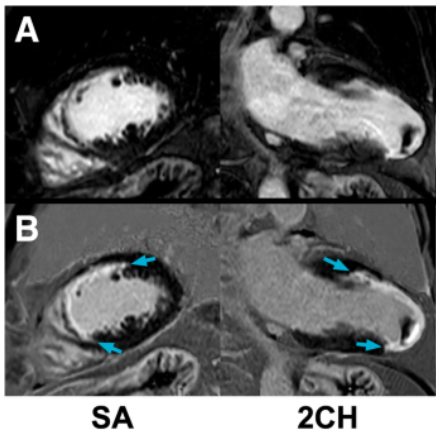

Figure 6: Bright-blood and dark-blood LGE imaging:

A: Bright-blood LGE images of SAX and 2CH (two-chamber) demonstrating myocardial infarction in the left anterior descending artery (LAD). The infarcted myocardium presents with a high signal intensity lesion in the image and infarction involves 75% to 100% of the myocardium. There is a thrombosis in the left ventricle blood pool which is presented with low signal intensity lesion (2CH).
B: Dark-blood LGE images of SAX and 2CH indicating myocardial infraction in LAD. The higher level of contrast between the infarcted area and blood in dark-blood LGE images makes subendocardial scar distinguishable (36).

1.2.1.3.2. LGE Images Analysis

LGE image analysis starts with evaluating the presence of LGE in these images visually. If LGE appears present in one view (short axis or long axis) or slice, it should be verified by cross-referencing with another view. This technique can increase the accuracy of identifying enhancement in late gadolinium enhancement imaging (34).

Various methods exist to quantify the myocardial fibrosis from LGE images such as thresholding based on standard deviations from the mean, or other techniques such as full-width half max (39).

Thresholding requires manual selection of normal myocardium as references. Pixels that have (n) standard deviation (SD) signal intensities away from the reference myocardium are defined as abnormal tissue (37) (38) **(Figure 7).** Various thresholding levels, such as 2SD, 3SD, 5SD, and 6SD, have been applied to quantify myocardial scar from LGE imaging (39).

The Society of Cardiovascular Magnetic Resonance (SCMR) Task Force on standardizing post reporting on LGE imaging in the assessment of ischemic fibrosis recommends a 5 SD threshold as appropriate for defining injury consistent with myocardial infarction or other scars (40) (41) (42) while a 3 SD threshold has been suggested for non-ischemic cardiomyopathy (43).

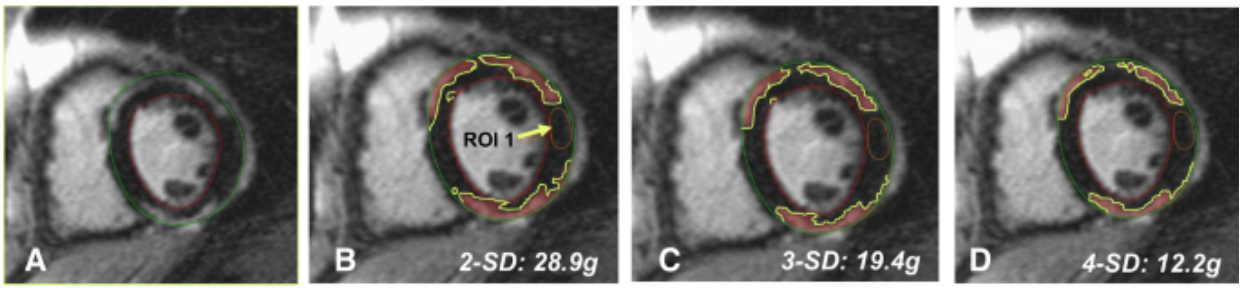

Figure 7*:* Different LGE thresholding methods for the assessment of scar in midventricular slice short axis (SAX) in a patient: The endocardium and epicardium contours are outlined by thin red and green lines, respectively (A). The region of interest (ROI) in the normal myocardium (demonstrated with the yellow arrow) is presented by an orange oval shape contour in the darkest area of the myocardium. The area of the myocardium with fibrosis (presented in red) is demarcated with yellow borders. 2-SD (B), 3-SD (C), and 4SD (D) were applied to quantify the fibrosis. SD= standard deviation (6).

The other method in scar assessment in LGE images is full-width half max, where all pixels with a signal intensity higher than 50% of the signal intensity (SI) of the scar are used to define damaged myocardium (44). This method has shown a high reproducibility since it is not affected by the surface coil signal intensity variation in gadolinium imaging (33) (37).

LGE imaging is a valuable approach in quantifying the scar burden to predict the mortality rate and assists clinicians in their clinical decision making and further management of the patients

(45) (46). LGE can quantify the scar in absolute values but also as a percentage of LV mass; for the latter, the value is calculated from the sum of enhancement from the LGE short axis (SAX) divided by the total left ventricular myocardial mass.

1.2.1.3.3 LGE Pattern

Late gadolinium enhancement is widely used as a diagnostic tool to assess the etiology of myocardial fibrosis, which can be an ischemic or non-ischemic cause**,** each of them has a specific distribution injury pattern (47) **(**48) **(Figure 8)**.

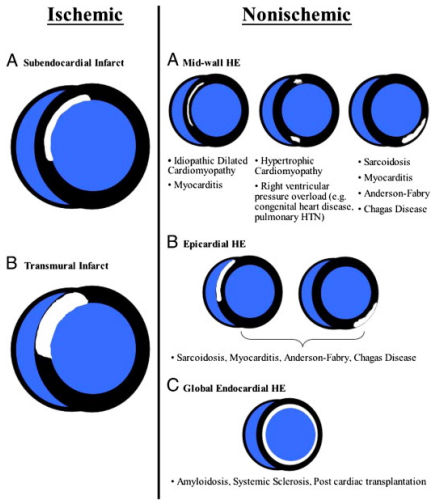

Figure 8: Different patterns of distribution of fibrosis: Ischemic and non-ischemic patterns (7): Ischemic injury can present as subendocardial or transmural. Non-ischemic injury typically appears with a mid-wall, subepicardial, or global subendocardial distribution pattern.

In ischemic injury, the regional distribution of myocytes reflects the tissue that is dependent on the culprit vessel, i.e., one or more of the three coronary artery territories (49). Each coronary artery supplies blood to a particular territory of the myocardium (49), with the Left Anterior Descending (LAD) artery blockage affecting the left ventricle's (LV) anterior portion and

interventricular septum and a left circumflex (LCX) blockage leading to fibrosis in the lateral LV wall, while a right coronary artery (RCA) involvement results in ischemic fibrosis in the posterior and inferior LV wall (75) (**Figure 9).**

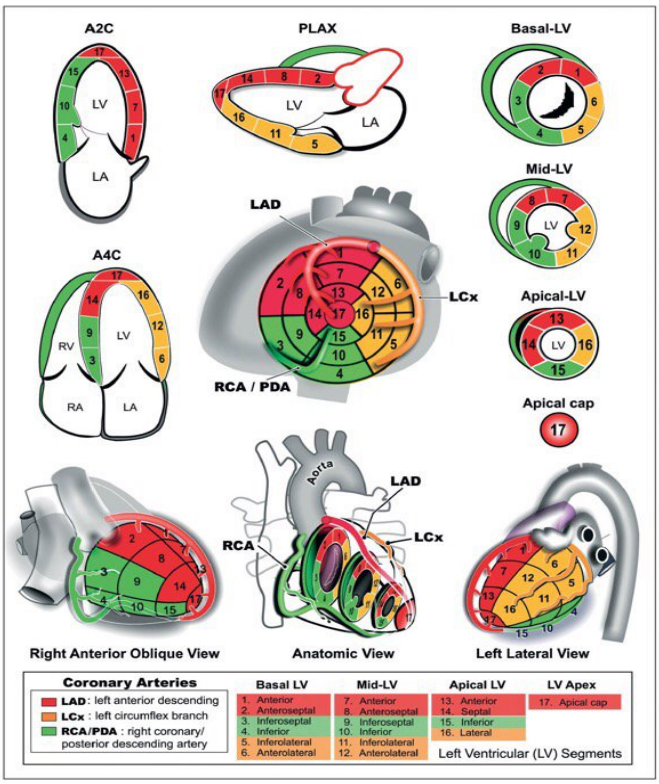

Figure 9: Coronary artery territories in different cardiac views: long axis (2-chamber, 3-chamber, 4-chamber view) and short-axis view. Left anterior descending artery (LAD), left circumflex (LCX), and right coronary artery (RCA). LAD supplies blood to the anterior and septal areas of the myocardium (red). LCX supplies blood to the lateral myocardial wall (orange). RCA provides blood to the inferior area of the myocardium (green) (8).

In no-flow ischemia caused by coronary artery occlusion, necrosis develops starting from the sub-endocardial layer, because it is more sensitive to hypoxia, partially because of oxygen demand (48). The volume affected by myocyte death expands in a wave-form pattern from the

endocardium to the sub-epicardium within approximately six hours after the onset of ischemia **(Figure 8).**

Depending on the duration of ischemia, the infarct can be confined to the sub-endocardial layer or, inter longer periods of ischemia involve the entire myocardial wall (transmural) including the subepicardial layer (48).

If the blocked coronary artery can be re-opened early, i.e., well before six hours of ischemia, the progression of the necrotic volume can be stopped (50), and then be subendocardial only (50).

In hypertrophic cardiomyopathy (CMP), dilated cardiomyopathy, and other non-ischemic causes of myocardial injury, various patterns of gadolinium distribution in the left ventricle can be observed. In non-ischemic CMP, the distribution pattern of injury typically is not that of a coronary artery territory and may include involvement of the mid-wall area only, insertion sites of the right ventricle, being patchy, or are subepicardial (49).

1.2.1.3.4 Clinical Impact of LGE Imaging:

As explained in the last section, LGE images display the etiology of the myocardial insult. LGE can visualize the regional distribution of the myocardial damage (48), such as a subendocardial or transmural myocardial injury in ischemic cases (48). This finding can help clinical decision-making in cases with unknown etiology of impaired cardiac function to understand better the specific pathophysiology of the patient (47)(48). LGE CMR typically has a high contrast between infarcted and normal myocardium and therefore can visualize scars with a sensitivity of as high as 92% (51).

LGE can provide valuable information about the infarct size in the myocardium in a patient with myocardial infarction (52), with high accuracy in histopathological validation studies (53). LGE imaging can visualize the extent of the scar and the remaining viable myocardium. The viable myocardium represents living tissue. Such tissue may however show decreased activity due to a mismatch in energy supply and demand. Viable myocardium may show contractile dysfunction (54). LGE can identify small areas of fibrosis which is prognostically relevant and can guide clinical decision-making concerning revascularization in patients after acute myocardial infarction (18)(19). In a coronary artery territory with a smaller area of necrosis, a greater improvement was observed after revascularization because of the larger viable myocardium in that region (55). The presence of LGE is also a predictor of arrhythmia, as gadolinium represents an expanded extracellular volume with the disturbing connection between myocytes. It was shown that LGE is a better identifier than other cardiac measurements such as left ventricular ejection fraction for estimating the risk for future arrhythmic events (56).

Different distribution patterns of ischemic scars have specific prognostic implications. A transmural extension of the scar has a poor prognosis in post-MI patient outcomes with a higher mortality rate (57) (58). A non-transmural distribution of necrosis or scarring has lower acute mortality but higher recurrence of MI (57)(59). A long-term follow-up of transmural vs non-transmural scars showed no significant difference in mortality (57). Recent studies demonstrated that even a small myocardial scar increases the risk of major cardiac events (60) (61).

Of note, LGE imaging may lead to a new diagnosis in 19% of patients and thereby change therapeutic management in 37% (62).

1.2.1.3.5. Shortcomings of Late Gadolinium Enhancement Imaging

Placing an intravenous catheter for injecting the contrast agent is a time-consuming and sometimes unpleasant experience which can lead to side effects including infection in the catheter insertion site. Contrast agents also add significant cost to the MRI exam (63).

Concerning the image acquisition, LGE is a semi-quantitative method (64)(65) that requires a trained operator to 'null' the magnetization level from the intact myocardium by identifying and applying the so-called inversion time to the MRI protocol, that is associated with a minimal signal of normal myocardium. This time varies between time points after the contrast agent injection, sequences and even between the right and the left ventricle. If the technician is not successful in identifying the correct time, the infarcted myocardium cannot be differentiated from the normal myocardium, and image analysis is not possible or extremely difficult (66).

A very considerable disadvantage of LGE is that it cannot detect diffuse fibrosis in myocardial diseases such as dilated cardiomyopathy. Since fibrosis may be evenly distributed in the myocardium, there is no 'normal' myocardium to refer to, making LGE less useful (67).

Gadolinium can lead to allergic reactions (68) and deposits in various tissues (68). Previously nephrogenic systemic fibrosis (NSF) with dermal and internal organs involvement (68) was considered to pose a significant risk to patients with acute renal failure or patients with severely impaired renal function (glomerular function rate <30 ml/min/ 1.73m2), although the recent statement of the American College of Radiology considers gadolinium application a low risk only in this population (69). Moreover, there are two structurally different categories of gadolinium chalets available for imaging- macrocyclic and linear structures. A macrocyclic gadolinium chalet

with a lower dose is recommended for safety reasons (72) to decrease the risk of gadolinium accumulation in the central nervous system and the epidermis (70)(71).

Gadolinium with toxic properties to cells, once released through urine and dissolved from the complex molecule used in medicine into its molecular form, may affect the environment and pollute ecosystems (73).

1.2.1.4. T1 and T2 Parametric Mapping*:*

The proton relaxation times T1 and T2 are fundamental markers for the magnetic properties of tissue. Their measurement by CMR mapping allows for a direct, quantitative assessment of myocardial tissue properties and helps identify tissue pathology in vivo (74), mainly associated to tissue water content or other molecular alterations in the myocardium (75).

CMR T1 mapping uses a series of images to reconstruct a map that displays myocardial T1 as a colour-coded map (70, 74) (**Figure 10).** Specifically, T1 equals the time until protons restate 63% of their equilibrium state (74).

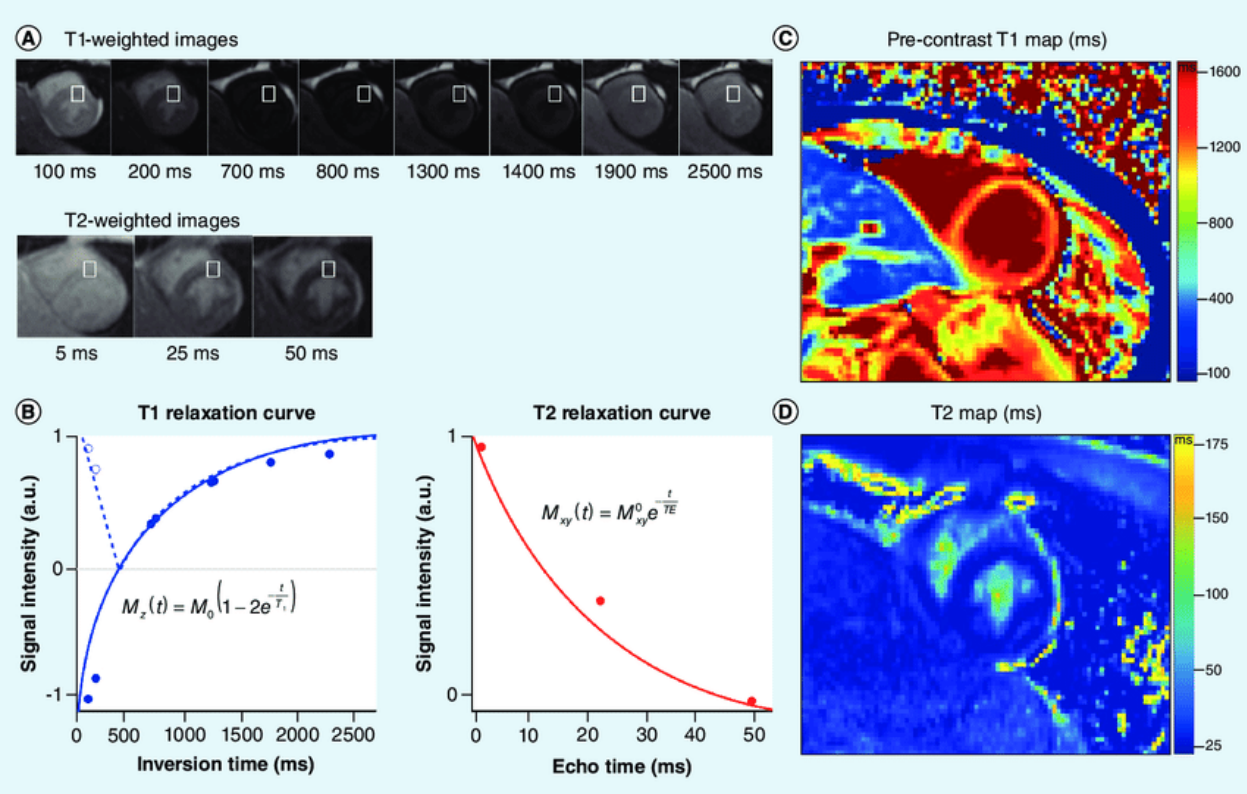

Figure 10: T1 and T2 mapping images: Source images with varying inversion times (A) are used to calculate the relaxation curves (B), from which T1 (C) and T2 (D) maps are calculated (from 9).

1.2.1.4.1. T1 Mapping:

T1 maps can be acquired using different magnetization preparation methods; the two most applied techniques are inversion recovery and saturation recovery sequences (76).

Saturation recovery sequences, based on multiple 90 degrees RF pulses, allow for faster image acquisition, while inversion recovery techniques use a 180-degree preparation pulse.

The available T1 mapping methods are different based on the image acquisition and the readout parameters and present different values (76). Two frequently used inversion recovery sequences are modified look locker inversion recovery (MOLLI) and short MOLLI (ShMOLLI). A frequently

used saturation recovery T1 mapping sequence is saturation recovery Single-shot Acquisition (SASHA) **(Figure 11**) (77).

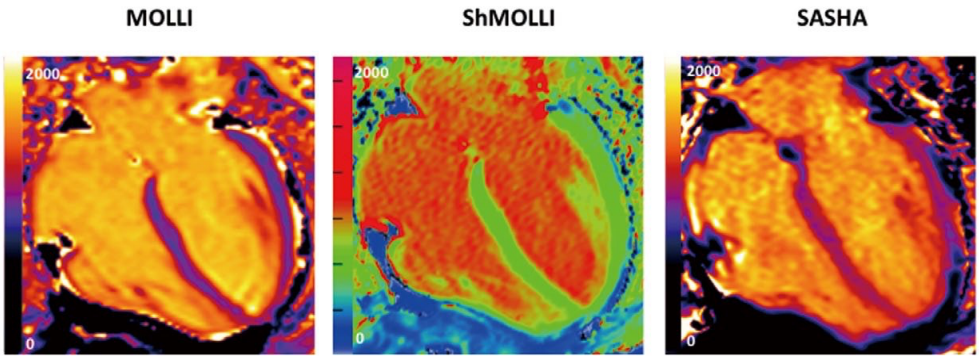

Figure 11: T1 maps from four chambers view from a healthy participant with three T1 map sequences (MOLLI, shMOLLI, SASHA; see text for details). Each method has its own range of normal values (136).

The first T1 mapping technique that was used was the Look-Locker sequence, which is still used for so-called TI scouts, which helps selecting a suitable inversion time to create the best contrast in LGE images (nulling of the myocardium). It includes an inversion pulse that prepares the longitudinal magnetization (78). Look-Locker is a long sequence with a long breath-hold, and it does not allow the magnetization to reach its equilibrium state, and therefore tends to underestimate T1 (79).

To reduce the error associated with Look-Locker sequences, a modified look locker inversion recovery (MOLLI) sequence was developed, within one breath-hold at the end-diastole of 17 consecutive heartbeats samples magnetization recovery after an inversion pulse (79). The common protocol for MOLLI is 5-(3)-3, which means during the first inversion recovery pulse five images are obtained, followed by a waiting period of 3 heartbeats to recover magnetization, and

3 image acquisitions thereafter. MOLLI is the most precise technique (i.e., with good reproducibility), but can underestimate T1 because of magnetization transfer and transverse magnetization effects (80)(81).

Magnetization transfer originates from the interaction between the bound protons in intracellular space and free protons in tissue water. The magnetization is exchanged between bound protons and free ones, thereby decreasing the observed signal (80)(81).

Another T1 sequence, the so-called short MOLLI (ShMOLLI), has a shorter breath holding time (9 heartbeats) when compared to MOLLI (17 heartbeats), making the image acquisition more comfortable for patients. On the other hand, ShMOLLI has less precision than MOLLI due to its incomplete recovery of magnetization recovery (77).

Saturation recovery single-shot acquisition has high accuracy. albeit with less precision (reproducibility) (77).

T1 mapping after gadolinium administration can be used to quantify the extracellular volume and thereby the extent of diffuse fibrosis using T1 maps acquired before and after gadolinium application (82), adding the hematocrit into an equation (83). This value is highest in acute myocardial infarction, and it is low in fatty accumulation and Fabry disease (**Figure 12).**

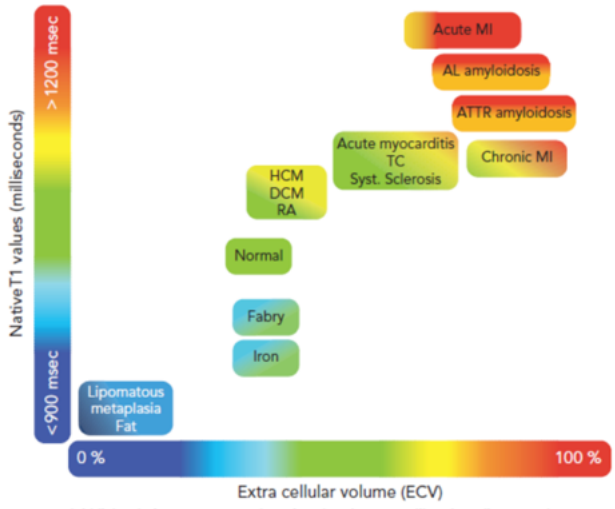

Figure 12: Selected myocardial diseases and associated abnormalities in native T1 and extracellular volume (ECV) derived from pre-and post-Gd T1: Certain tissue pathologies associated with myocardial diseases show predictable changes in T1 and ECV that can be used for diagnostic purposes. For example, acute MI has very high T1 and ECV values, while low T1 values with low-normal ECV are found in Fabry's disease and iron accumulation. The color code that is presented in this graph can help to visualize the myocardial changes (10).

1.2.1.4.2. T2 Mapping:

T2 mapping is based on a series of images that allow for estimating the transverse relaxation time. While T2-weighted images are sensitive to water-bound protons by showing a higher SI in tissue with increased water content, T2 maps measure the transverse relaxation time and can display tissue with higher water content by the associated longer T2, which typically is indicative of acute myocardial injury (84).

1.2.1.4.2.1. Edema Imaging:

T2-weighted sequences can be applied to identify edema in the myocardium. It has some limitations, including a variable signal intensity related to an inherently low signal-to-noise ratio,

coil sensitivity field inhomogeneities, high signal intensity from slow-flowing blood in the ventricle, and sensitivity to flow and arrhythmia-related artifacts. Such issues may make it challenging to identify subendocardial injury or subjectivity of this method. T2 mapping can identify myocardial edema without these limitations (85).

Acute myocardial injury is associated with a rapid (within less than 30 minutes) onset of edema after the onset triggering event (e.g., ischemic injury due to coronary artery occlusion, viral infection, or transplant rejection (86).

Two types of T2 mapping sequences are being used: Dark blood turbo spin-echo and bright blood T2 preparation pulse-based sequences**.** The Turbo spin-echo technique can cause ghosting artifacts from blood flow that causes signal loss which makes it not an appropriate sequence for clinical assessment (87). T2 preparation-based approaches are not affected by this limitation and can be produced by adding a T2 preparation pulse to a sequence like balanced SSFP or rapid gradient echo. The T2 preparation pulse can be a 90-degree or 180-degree RF pulse.

1.2.1.5. Parametric Mapping Image Analysis:

Mapping has the potential to detect changes in tissue components which helps to assess tissue pathology, including the focal changes or diffuse ones (88).

A normal reference value is required to differentiate the damaged myocardium from the normal myocardium, but contrary to LGE, the normal reference value from the same individual's myocardium is not utilized. Because measured T1 or T2 values are different between different field strengths as well as scanner make and model, local normal values based on healthy volunteers need to be established (89). Healthy volunteers should not have any medical

condition, be free from cardiovascular symptoms, have a normal ECG, normal cardiovascular function, and no evidence for tissue abnormalities in CMR (88).

The normal values of healthy volunteers are used to define normal and abnormal and used to create a colour scale map for a visual presentation of myocardial tissue abnormalities (**Figure 12).**

1.2.1.5.1. Variability in Parametric Mapping Values:

There are various imaging and biological factors that affect mapping values. Mapping results from a patient should be reported based on the sequence- and scanner-specific normal range. These values can also be affected by the software version of the scanner, or the software used for evaluation.

The other factor that affects mapping values is the magnetic field strength; T1 is longer at higher field strengths (75) (90), while T2 is shorter at higher field strengths (87).

Moreover, mapping is dependent on physiological confounders, such as heart rate variations (90), mainly the time between inversions. More recently developed T1 sequences such as shMOLLI are less dependent on variations of heart rate, with improved accuracy (91). Also, the sensitivity of MOLLI to heart rate changes decreases with the sampling modification such as the 5(3)3 (91).

Some studies reported age and sex influence mapping values; for instance, the T1 mapping value increases with increasing age in males but not in females. Age-related interstitial fibrosis found in histopathology studies may explain the observed increased T1 in older men (92). For T2 mapping values, healthy female volunteers presented higher T2 values than male participants, Additionally, older volunteers had increased T2 values (94). However, not all studies supported the age factor in mapping values. (93).

T1 and T2 mapping have the potential to identify myocardial tissue abnormalities that have a significant diagnostic value (88).

1.2.1.6. Native Parametric Mapping in Acute and Chronic Myocardial Infarction:

In acute ischemic events, native mapping values are increasing during the first hours after the ischemic injury due to direct cellular injury (loss of cell membrane function) and the inflammatory response, all leading to an increase in the myocardial water content (82). Myocardial T2 appears to increase in acute injury even before cardiac-specific inflammatory enzymes (troponin) increase (95). T2 mapping values can identify the area at risk of acute myocardial injury and differentiate irreversibly (necrosis) and reversible damage (salvageable or salvaged myocardium) (96).

In myocardial infarction, T1 values reach a peak level 8 to 14 days after an ischemic event. T1 values are expected to decrease again to a new baseline over 6 months, based on the injury's extension and severity (82). The large area of myocardial injury with elevated mapping values in the acute phase is undergoing replacement fibrosis resulting in a much smaller area with solid fibrosis which has been identified with higher T1 values than the normal myocardium (97).

An increase in T2, sensitive to edema (98), in acute myocardial infractions can differentiate between acute and chronic myocardial infarcts.

In chronic ischemic fibrosis, the expansion of the extracellular space leads to an increase in the T1 value (99) (100) (101). However, chronic ischemia assessment with native T1 value should be done cautiously since fatty degeneration in chronic fibrosis can result in pseudo-normal T1 values in that area (102) (103).

1.2.1.7. Clinical Implications of Parametric Mapping:

Parametric mapping is still not widely distributed and requires more standardization and validation. Mapping is used in many centers complementary to LGE imaging or when LGE cannot identify fibrosis, such as in diffuse cases (104). In dilated cardiomyopathy and hypertrophic cardiomyopathy, the native mapping may be more sensitive to identifying abnormal myocardium than LGE imaging (105).

Mapping is a quantitative technique with long-term stability and high reproducibility in terms of values, which are essential in clinical practice for patient management and follow-up (106) (107) (108) (109). In healthy volunteers, myocardial T1 was shown to be stable over time, even over a follow-up of more than 3 years (106).

The ability of T1 mapping to correctly identify the location and extent of fibrosis has been validated, demonstrating good agreement with histopathological studies in animals and humans (110) (111).

Native mapping is a fast-imaging method compared to LGE for tissue characterization since there is no need to insert an intravenous catheter to inject the contrast agent and wait for 10 minutes to visualize the scar with the contrast medium after its injection. It is also a simpler method as the optimal sequence parameters are mostly standardized.

Native mapping can establish a diagnosis for acute myocardial injury by identifying the area with reversible injury and predicting functional recovery (112). The native T1 value is reported to

predict the major cardiac events such as all-cause mortality better than other CMR criteria in acute injury (102) (113) (114).

In chronic cases, native T1 mapping has shown a 95% sensitivity and 97% specificity in identifying myocardial fibrosis (115). A recent study showed that native T1 and T2 have an excellent diagnostic accuracy in identifying acute and chronic myocardial infarction (AUC 0.975 and 0.979, respectively). The value of native T1 and T2 mapping decreased dramatically in a follow-up CMR scan at 6 months (P<.0001) (115).

1.2.1.8. Shortcoming of Parametric Mapping:

Although useful, parametric mapping has limitations that hamper clinical adoption. Conventional mapping extracts one parameter (T1, T2) at a time and requires patients to breathe in and hold their breath to acquire each image, leading to long scan times (75). The shorter the period of holding breath, the better patients can tolerate this method, which is especially important in elderly and clinically very sick patients (116). For various T1 mapping techniques, breath-holds with a length of 17, 11, and 9 heartbeats have been used (108). Usually, the imaging technicians instruct the patient on breath-holding during image acquisition to decrease the effect of the chest movement on image quality (75).

Interpretation of mapping values is dependent on the normal values established from the healthy volunteers for each sequence and scanner (see above). Various criteria for defining a healthy population are being used and may affect the comparability of results between centers (88).

The other limitation of mapping is the absence of a standardized reporting system for mapping parameters; it is not feasible to compare the mapping values from one site to another site (117) (118). A solution for a standardized reporting system of the mapping technique could be the use of Z scores. With this biostatic value (119), myocardial mapping values are presented normalized to the local normal reference values. Z scores are not susceptible to the known confounders and allow for using the same values on all scanners (118) (120). The method was validated in amyloidosis patients and normal participants in 1.5T and 3T scanners (118).

1.2.1.9. Future of Parametric Mapping*:*

Despite the limitations of mapping, native mapping is a developing field in quantitative CMR with its novel approaches such as fast acquisition and free-breathing sequences, all with a significant potential compared to the conventional mapping techniques.

Free-breathing acquisitions are being developed and may improve map quality, especially in patients with shortness of breath (121).

New emerging methods such as fingerprinting CMR, which can simultaneously acquire T1 and T2 values may have shorter acquisition times and shorter breath-holds (90) (122).

Another novel sequence, MR Multitasking with free breathing may further simplify scanning by introducing simultaneous multi-parametric acquisition, reconstruction, and evaluation (123).

Such high dimensionality and highly under sampled patch-based reconstruction techniques allow for reducing the amount of required raw MR data and may allow for the acquisition of parametric mapping in a reduced scan time while keeping a high image quality (124).

1.3. Thesis Objectives:

Native T1 and T2 mapping may have the potential to be applied in routine clinical imaging for myocardial tissue characterization.

The objective of this study was to assess the agreement between the native mapping and LGE in ischemic cardiomyopathy patients to identify the presence, pattern, and extension of the myocardial injury.

CHAPTER 2

2. METHOD

2.1. Population Selection

This retrospective study has approval from the institutional research board of the McGill University Health Centre (REB#2021-7566) to recruit patients with a diagnosis of ischemic cardiomyopathy from an ongoing study called CMR10, who underwent a clinically indicated CMR scan between December 12, 2019, and December 31, 2020.

The inclusion criteria for this study are presented in table 1. Participants needed to be 18 years old or older have written informed consent and have documented ischemic cardiomyopathy diagnosis based on their CMR report (**Table 1).**

Normal mapping values were obtained from a cohort of healthy volunteers, scanned on the same scanner at the McGill University Health Centre.

Table 1: Inclusion and exclusion of participants in this study

Inclusion Criteria	Exclusion Criteria
Age> 18 years	General MRI contraindications (pacemakers, claustrophobia, implanted devices, pregnancy, etc.)
Informed Consent as documented by signature	T1/ T2 mapping or LGE images not performed
Documented ischemic cardiomyopathy diagnosis based on the cardiac MRI	Poor CMR image quality

2.2. Baseline Clinical Characteristics

Baseline clinical characteristics of the participants such as resting heart rate and resting systolic/ diastolic blood pressures, gender, age, body mass index, and body surface area were extracted from each participant.

2.3. CMR Protocol and Image Analysis

2.3.1. CMR Protocol

CMR scans were conducted on one of three different scanners: 1.5 T Signa Artist (GE Healthcare, Milwaukee, Wisconsin, USA), 3T Skyra (Siemens Healthineers, Erlangen, Germany) and 3T Premier (GE Healthcare, Milwaukee, Wisconsin, USA), all at the MUHC site.

A standard fibrosis protocol was used which comprised the following sequences (**Figure 15**):

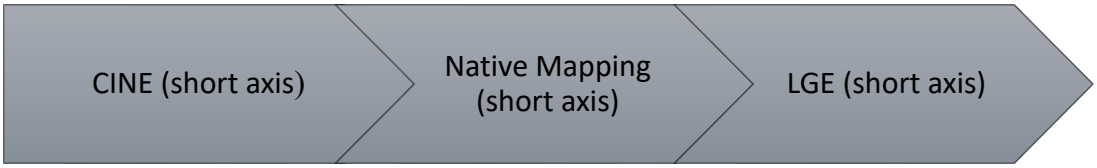

Figure 13: CMR protocol phases.

All images were captured at end-expiration during a breath-hold period.

Gadobutrol (Gadovist™) (0.1mmol/kg) was used as a contrast agent for LGE imaging. It was injected using a peripheral intravenous (IV) access. Seven minutes after gadolinium injection, LGE images by acquired with selecting an inversion time (TI) that can differentiate the blood pool from dark myocardium.

2.3.2. Pulse Sequence Description

The pulse sequences for cine images included a Steady-State Free Precession acquisition (Free Imaging Steady State, FIESTA for the 1.5T and 3T MRI GE systems, and True Steady state free Precession (TruFISP for Siemens). 2, 3, and 4 chambers long axis (LAX) and short-axis images (SAX) were acquired.

Table 2 demonstrates the T1 sequence parameters for T1 mapping for each scanner. A MOLLI 5(3)3 scheme was used for T1 mapping in all three scanners.

Table 2: T1 map sequence characteristics in GE 1.5T, GE 3T, and Siemens 3T: For all T1 mapping sequences, a MOLLI sequence was applied *and*

	GE 1.5T	GE 3T	Siemens 3T
Pulse sequence	MOLLI 5,3,3	MOLLI 5,3,3	MOLLI 5, 3,3
Field of view	360x360	360x360	360x360
TE	1.29	1.36	1.12
Slice thickness	8mm	8mm	8mm

LGE images were acquired with the parameters included in **Table 3** for each scanner. Gradient echo sequence was used on all three scanners for acquiring LGE images.

Table 3: Selected LGE image sequence parameters for the three scanners:

	GE 1.5T	GE 3T	Siemens 3T
Pulse sequences	Gradient echo	Gradient echo	Gradient echo
Slice thickness	8mm	8 mm	8mm
Flip angles	25	45	20

The T2 mapping sequence for GE scanners was Fast Spin Echo (FSE), and True Fast Imaging steady-state free precision (TRUFI) for the Siemens scanner (Table 4).

Table 4: T2 map sequence characteristics for GE 1.5T, GE 3T, and Siemens 3T scanners. The sequence is called fast spin-echo for GE scanners and is called Trufi steady-state free precession) for the Siemens scanner.

	GE 1.5T	GE 3T	Siemens 3T
Pulse sequences	Fast Spin Echo	Fast Spin Echo	TruFISP
Slice thickness	8mm	8 mm	8mm

2.3.3 Image Analysis

2.3.3.1. Baseline assessment of CMR Image Quality:

The LGE images and maps were assessed visually for the presence of artifacts. Such artifacts can be caused by cardiac motion, breathing motion, arrhythmia, or a partial volume effect of volumes with a mix of blood and myocardium, (106) (125). Since artifacts typically impair image quality and thereby result accuracy, images with artifacts were excluded from the study (107).

2.3.3.2. CMR Image Analysis tool and technique

A clinically certified software, (CVI42 version 5.11.4, Circle Cardiovascular Imaging Inc., Calgary, AB, Canada) was used for CMR image analysis and reporting. The software includes a tissue characterization module to semiautomatically quantify fibrosis in LGE and mapping images**.**

The slice location as retrieved from the DICOM header information and anatomical landmarks such as papillary muscles and right ventricle insertions to the left ventricle from the maps and LGE images were used as a guide to verify the location of corresponding slices (**Figure 14).**

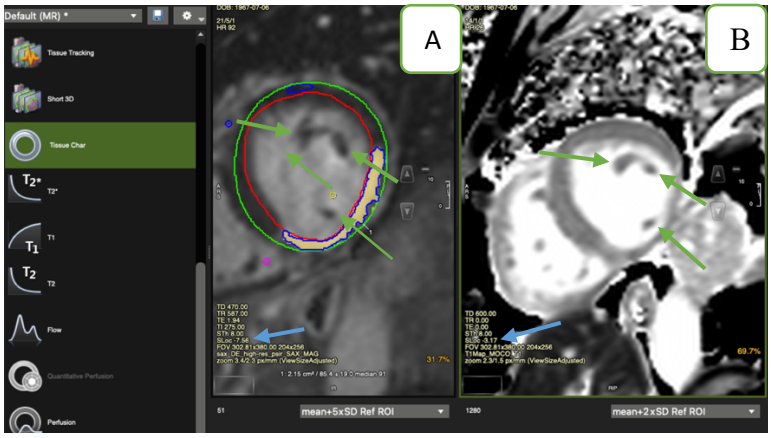

Figure 14*:* Corresponding LGE image and T1 map images as verified by slice location and anatomical landmarks: Images from a patient basal slice of short-axis (SAX) view of LGE image (image A) and T1 map (image B). The blue arrow presents the slice location (SLOC) from the DICOM header which is -7.56 in LGE image and -3.17 in T1 map. The green arrows show similar anatomical landmarks which are the papillary muscles in these two images. The small differences between images are due to a small difference in the cardiac cycle (the time after the R wave/TD varies by 130ms).

Three slices (apical, mid, and basal) (**Figure 15**) for each patient from LGE and T1 maps were paired together based on their anatomical landmarks such as trabeculation and pupillary muscles and slice location (**Figure 14**).

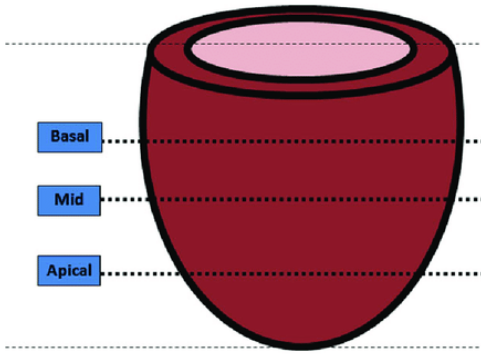

Figure 15: Slice selection in the cardiac tissue CMR imaging: Presenting the location of three slices (dotted lines) in left ventricles (apical, mid, and basal) (11).

Segmentation of the myocardium: The subendocardial and subepicardial borders were drawn manually in short axis LGE images. The subendocardial border separates the myocardium from the blood pool. The subepicardial border separates the myocardium from the right ventricle and the pericardium. (**Figure 16**).

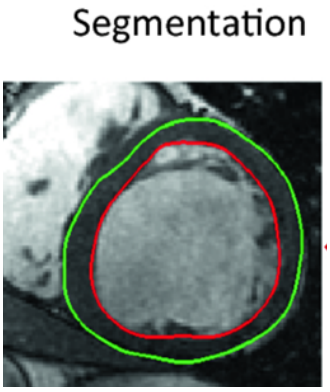

Figure 16*:* Segmentation of the short axis view in the mid-ventricular slice of the cardiac tissue: The green line represents the subepicardial contour; the red line represents the subendocardial contour (12).

The subendocardial and subepicardial borders defined the left ventricle myocardium for the image analysis software for further assessments. Great care was taken to exclude the blood pool or epicardial fat (110). Two experienced cardiologists validated the segmentation in a randomly selected 10 samples.

In the first part of the experiment, the LGE images were analyzed as the ground truth technique for irreversible myocardial injury as validated in animal and human histopathologic studies (126).

We used a standard deviation (SD) based method to automatically identify infarcted myocardium. After drawing a region of interest in the reference myocardium (with low signal intensity), the software automatically displays the myocardium with the signal intensity of 5SD above the mean signal of this reference and marks it as yellow (152) (**Figure 17).**

In LGE images, the border of the area with enhancement which represented the myocardial injury was then manually demarcated. The resulting contour was copied to the corresponding T1 image (grayscale map) to the same anatomical location (**Figure 17)**.

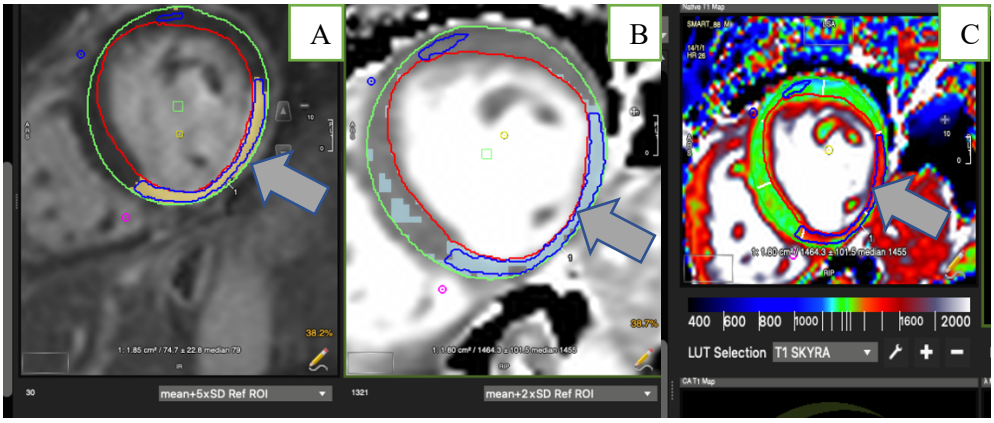

Figure 17*:* Assessment of the location of the myocardial injury (thick arrow) in different tissue characterization images: These three images were from the same patient. All images represent fibrosis in the same location. A: LGE image: The yellow-colored area presenting fibrosis was demarcated with the blue line. B: T1 map grayscale: The blue area demonstrated the area with elevated mean T1 value, while the contour represents the manually drawn contour pasted from the LGE image. C: Color-coded T1 map: The red area inside the myocardium was the area with an elevated mean value.

The resulting mean T1 value was measured and compared with the normal value range of T1 for each scanner. If the mean T1 value of the area was higher than the mean+2SD (127) of healthy volunteers for the scanner, the area was considered an area with an elevated T1 value.

In the second part of the experiment, the T1 map colour scale for visualizing the mapping values in the myocardium was applied as the ground truth technique instead of LGE images. The green colour presented normal myocardium which had the mean T1 values in the range of mean T1 value ± 2SD of the normal healthy volunteers. Red represented the values that were higher than the normal values. Blue presented the myocardium with T1 values lower than found in normal myocardium.

A contour surrounding the area of increased T1 was manually drawn and pasted to the corresponding LGE images. The presence or absence of enhancement in the LGE image in the same area identified as a high T1 value was documented.

Finally, the T2 images were paired with LGE images that identified the same area of myocardial injury in the T1 map. The contoured area that was identified in LGE and T1 mapping images as myocardial injury were copied and pasted to T2 map images. The mean value of the T2 map in the area was recorded. The elevated T2 value was defined as the mean T2 values above 2 SD of normal healthy volunteer values. The presence or absence of abnormal T2 values and their area were recorded (**Figure 18).**

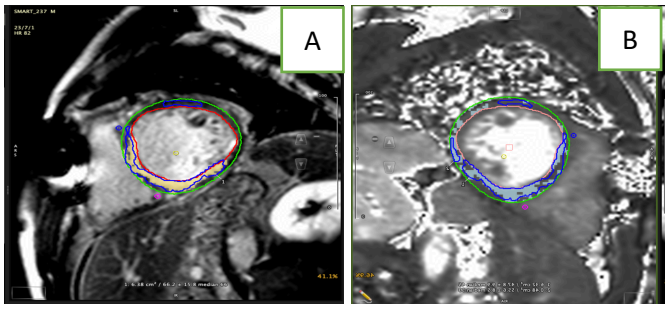

Figure 18: Assessment of the presence of myocardial edema in the same location where LGE identified myocardial injury: A. LGE image short-axis views: The areas of the abnormal signal are represented by a yellow (A) and blue (B) colours. The subendocardial, subepicardial and the enhancement extent contours were copied from LGE image (A) and pasted to the T2 map (B).

2.4. Data Analysis

CMR images and demographic data were retrieved from study records. Data analysis was performed with Microsoft Excel (Baton Rouge, United States) and SPSS (Chicago, United States). The normal distribution of the data was assessed with the Kolmogorov- Smirnov test (128). Normally distributed data were expressed as mean ± SD and were compared with the student T-test. Non-parametric (not normally distributed) data were presented as median with interquartile (IQR) and compared with the Wilcoxon rank test (41). A p-value of less than 0.05 was considered significant.

The kappa value was used to assess the degree of agreement between LGE and native mapping in identifying the myocardial injury (129) (**Table 5).** The intra-class correlation coefficient was used to evaluate the inter-observer variability between two blinded observers in assessing T1 and LGE images (129) (130). The McNemar test was used to assess the agreement between LGE and T1 map images in identifying the area of the myocardial injury based on the American Heart Association (AHA) segmentation (131).

Table 5: Interpretation of Cohen Kappa: Demonstrating the different values of Kappa and the level of agreement (129).

Value of Kappa	Level of Agreement	% of Data that are Reliable
0–.20	None	0–4%
.21–.39	Minimal	4–15%
.40–.59	Weak	15–35%
.60–.79	Moderate	35–63%
.80–.90	Strong	64–81%
Above.90	Almost Perfect	82–100%

CHAPTER 3

3. RESULTS

3.1. Cohort selection

Of the 46 patients who were diagnosed as having ICMP on their CMR report between December 12, 2019, to December 31, 2020, six patients were excluded: two of them were missing LGE images, and four patients were missing T1 mapping images.

LGE and T1 mapping images from 40 patients were matched based on slice location (SLOC) visualized from the DICOM header and checked by anatomical landmarks in the images themselves. Of the remaining 40 patients in the study, eight patients were excluded because the anatomical landmarks in the LGE and T1 mapping images did not match. The mean age of the 32 remaining participants was 64 years. Nine percent were female (only 2 female participants).

The basic clinical and CMR characteristics of patients and healthy volunteers are presented in table 6.

Table 6: Clinical and CMR characteristics of patients and healthy volunteers:

	Patients	Healthy volunteers	
Participant's characteristics			
Number of participants	32	28	
Male	30 (93.75%)	19 (54.28%)	
Age (year)	64±13	42±15	<0.0001 *
Body mass index (BMI)	26.77±5.16	24.21± 2.88	0.001 *
Body surface area (BSA)	1.94±0.21	1.85± 0.208	0.10
Comorbidities			
Diabetes mellitus	10 (31.25%)	0	
Hypertension	24 (75%)	0	
Smoking	8 (25%)	0	
Ventricular function (CMR findings)			
LVEDV (ml)	157.04±56.63	146.91±41.48	0.438

LVESV (ml)	90.5±58.63	52.96±26.29	0.0028*
LV EF (%)	47.31±17.44	67.78 ±8.59	<0.0001 *
SV (ml)	63.56±17.73	100.14±21.14	<0.0001 *

LV= left ventricle, ESV= end-systolic volume, EDV= end diastolic volume, EF= ejection fraction, SV=stroke volume, (*) p value<0.05

3.2 Normal Mapping Values

Healthy volunteer data were acquired from 28 participants with a mean age of 42± 15 (54% male, Table 6). Their CMR data values served as the normal T1 and T2 mapping values (Table 6). For basal slices, the mean T1 mapping values were 1000.34± 32.38, 1165.13± 39.64, and 1202.11± 34.98 for GE Artist (1.5T), GE Premier (3T), and Siemens Skyra (3T), respectively. For mid-ventricular slices, the mean T1 mapping values were 1008.14± 32.29, 1175.34± 34.75, and 1212.86± 33.3 for GE Artist (1.5T), GE Premier (3T), and Siemens Skyra (3T), respectively. For apical slices, the mean T1 mapping values were not estimated in healthy volunteers, the global values were used for apical slices. In apical slices, the partial volume effect can impair image analysis and lead to errors in the interpretation of the mapping results (125). The mean T1 mapping values were 1004.24± 31.41, 1170.24± 35.57, and 1207.49± 30.55 for GE Artist (1.5T), GE Premier (3T), and Siemens Skyra (3T), respectively.

The pathologic values for each scanner were presented in **Table 7**. 2SD above mean was used to define pathological tissue.

For basal slices, the mean T2 mapping values were 50.59±3.54, 44.95±4.01, and 39.19±2.50 for GE Artist (1.5T), GE Premier (3T), and Siemens Skyra (3T), respectively. For mid-ventricular slices, the mean T2 mapping values were 51.85± 4.12, 45.07± 3.57, and 40.62± 2.80 for GE Artist (1.5T),

GE Premier (3T), and Siemens Skyra (3T), respectively. For apical slices, the mean T2 mapping values were not estimated in healthy volunteers, the global values were used for apical slices. The mean T2 mapping values were 51.22± 3.59, 45.01± 3.60, and 39.91± 2.42 for GE Artist (1.5T), GE Premier (3T), and Siemens Skyra (3T), respectively.

For basal slices, the 2SD above the mean T1 mapping values were 1065.1, 1244.41, and 1274.12 for GE Artist (1.5T), GE Premier (3T), and Siemens Skyra (3T), respectively. For mid-ventricular slices, the 2SD above the mean T1 mapping values were 1072.72, 1244.84, and 1279.46 for GE Artist (1.5T), GE Premier (3T), and Siemens Skyra (3T), respectively. For apical slices, the pathologic values were 1067.06, 1241.38, and 1268.59 for GE Artist (1.5T), GE Premier (3T), and Siemens Skyra (3T), respectively.

For basal slices, the 2SD above the mean T2 mapping values were 57.67, 52.97, and 44.19 for GE Artist (1.5T), GE Premier (3T), and Siemens Skyra (3T), respectively. For mid-ventricular slices, the 2SD above the mean T1 mapping values were 60.09, 52.21, and 46.22 for GE Artist (1.5T), GE Premier (3T), and Siemens Skyra (3T), respectively. For apical slices, the global values have been applied, where the pathologic values were 58.40, 52.21, and 44.75 for GE Artist (1.5T), GE Premier (3T), and Siemens Skyra (3T), respectively.

Table 7: Mapping values of healthy volunteers for each scanner used in this study: This table presents the normal mean, standard deviation (SD), and 2SD of T1 and T2 mapping values of healthy volunteers in basal, mid-ventricular, and global left ventricular slices

Scanner 3.0 T Siemens			
Slice/mapping parameter	Mean	SD	Mean± 2SD
Basal T1	1202.11	34.98	(1132.15, 1274.12)
MID T1	1212.86	33.3	(1146.26, 1279.46)
Global T1	1207.49	30.55	(1146.39, 1268.59)

Basal T2	39.19	2.50	(34.10, 44.19)
MID T2	40.62	2.80	(35.02, 46.22)
Global T2	39.91	2.42	(35.07, 44.75)
Scanner 3.0 T Premier			
Slice/mapping parameter	Mean	SD	Mean± 2SD
Basal T1	1165.13	39.64	(1085.85, 1244.41)
MID T1	1175.34	34.75	(1105.84, 1244.84)
Global T1	1170.24	35.57	(1099.1, 1241.38)
Basal T2	44.95	4.01	(36.93, 52.97)
MID T2	45.07	3.57	(37.93, 52.21)
Global T2	45.01	3.60	(37.81, 52.21)
Scanner 1.5 T Artist			
Slice/mapping parameter	Mean	SD	Mean± 2SD
Basal T1	1000.34	32.38	(935.58, 1065.1)
MID T1	1008.14	32.29	(943.56, 1072.72)
Global T1	1004.24	31.41	(941.42, 1067.06)
Basal T2	50.59	3.54	(43.51, 57,67)
MID T2	51.85	4.12	(43.61, 60.09)
Global T2	51.22	3.59	(44.04, 58.40)

3.3. LGE imaging and mapping paired slices

Pairwise analysis of the presence of myocardial fibrosis was performed between LGE images and T1 maps. In total, 18 apical, 25 mid-ventricular, and 29 basal slices were compared. Five patients had their CMR exams on the Siemens scanner, seven on the 1.5T GE scanner, and 20 on the 3T GE scanner.

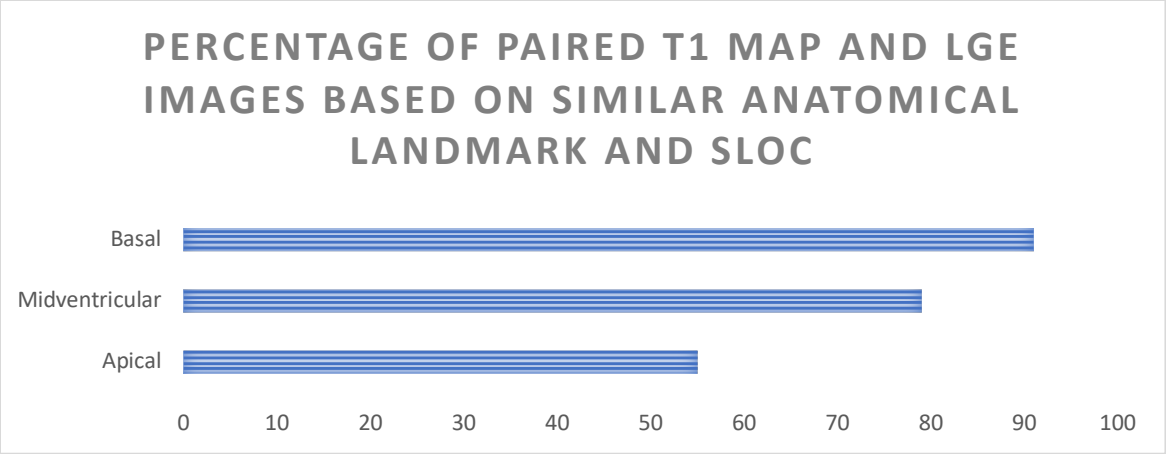

Figure 19*:* Percentage of paired T1 maps and LGE images in apical, mid-ventricular, and basal slices based on similar anatomical landmarks and slice location. Of 32 patients, 29 (91%) had paired images in basal, 25 (78%) in mid-ventricular, and 18 (55%) in apical slices.

Figure 19 shows the number of all T1 maps and LGE slices assessed: 18 apical, 25 midventricular, and 29 basal slices.

All 29 basal slices had elevated T1 values, while 28 showed areas with enhancement in the LGE images. Of all 29 basal slices, 24 had elevated T1 values in the same area of enhancement as the LGE images.

All analyzed 25 mid-ventricular slices had elevated T1 values, while 23 slices showed areas with enhancement in the LGE images. From these 25 slices, 22 had elevated T1 values in the same area of enhancement as the LGE images.

In the 18 analyzed apical slices, 15 had elevated T1 values, while 17 showed enhancement in LGE. From these 18 slices, 13 had elevated T1 values in the same area of enhancement as the LGE images (**Figure 20).**

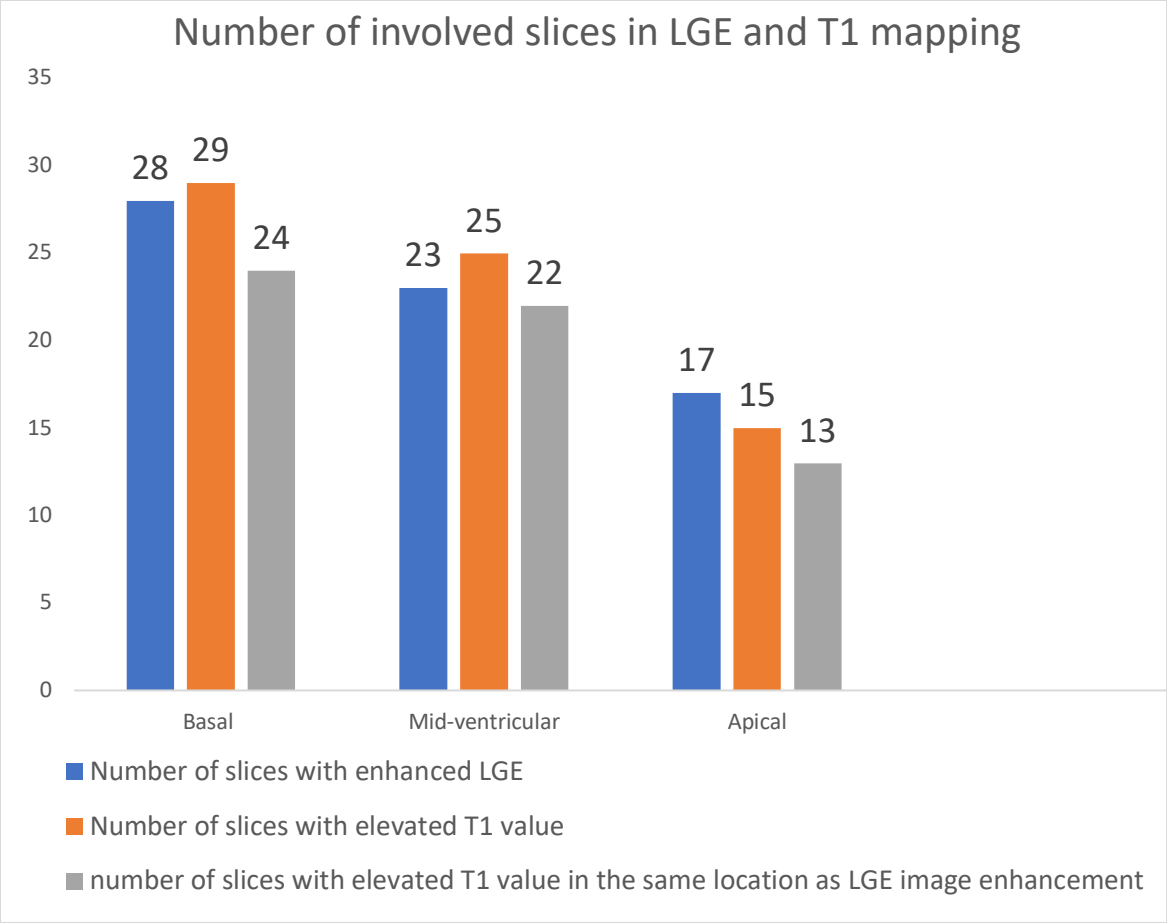

Figure 20: The number of slices showing myocardial injury, separated by slices and method of detection. Percentage of the slices with enhanced LGE (blue), elevated T1 value (brown), and elevated T1 value in the enhanced area identified by LGE (orange) from the total number of applied slices. 24 (82.5%) basal slices had elevated T1 values in enhanced LGE images. 22 (88%) and 13 (72.22%) mid-ventricular and apical slices, respectively had the same area of myocardial injury in T1map as identified in LGE images.

T1 maps of five (20.83%) basal slices, three (13.64%) mid-ventricular slices, and two apical slices (15.38%) with an area indicating a myocardial injury that was not present in LGE images **(Figure 21) (Figure 22).**

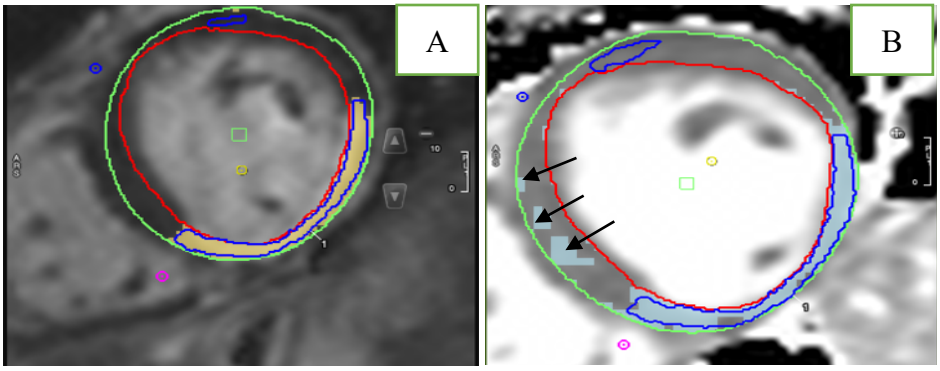

Figure 21T1 map identifies other areas of myocardial injury than the LGE images. The SAX images from the LGE images (A) and T1 map (B). The black arrows in the T1 map image (B) demonstrates the tissue damage that T1 map detected, but LGE imaging does not identify them.

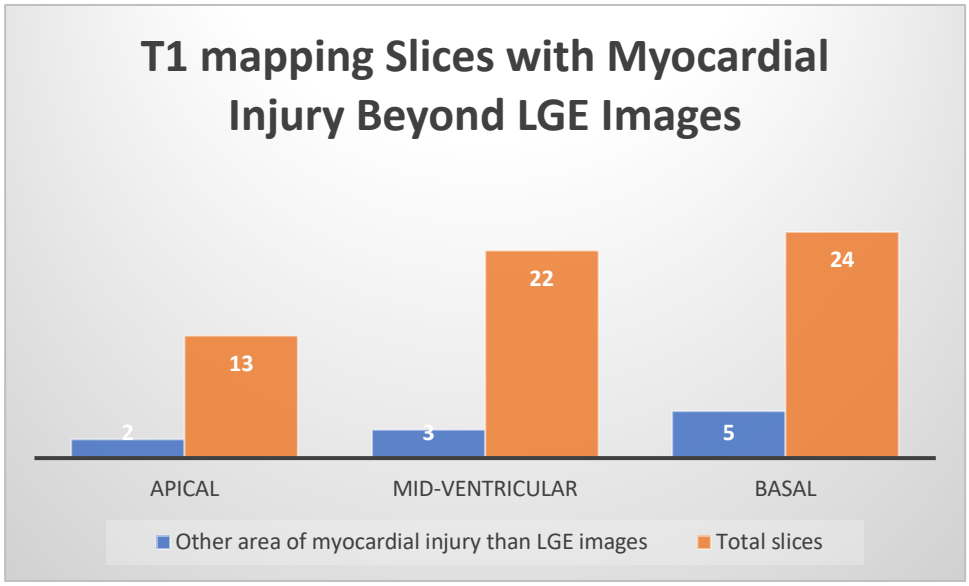

Figure 22: T1 maps with additional areas of myocardial involvement when compared with LGE: Number of apical, mid-ventricular, and basal slices with elevated T1 but without abnormal LGE.

3.4. Identifying the presence of myocardial damage by CMR imaging

3.4.1. Identifying the presence of myocardial damage as identified by the LGE images

All results in this section are reported with LGE imaging as the ground truth technique to identify tissue damage in T1 maps. The level of agreement between LGE images and T1 maps in identifying myocardial injury is demonstrated in **Table 8.** An excellent kappa coefficient of the agreement was observed in mid-ventricular and basal slices (kappa coefficient of 0.93 and 0.87, respectively). Apical slices had a moderate agreement with a kappa coefficient value of 0.66.

Table 8: Kappa agreement in identifying myocardial injury in T1 mapping based on LGE images: Agreement in identifying myocardial injury between T1 maps and LGE. Basal and mid-ventricular slices show the best agreement.

Identifying fibrosis	Apical	Mid-ventricular	Basal
Measure of agreement from LGE to T1 map	**0.66**	**0.93**	**0.87**

The sensitivity, specificity, positive predictive values, and negative predictive values for native T1 mapping to identify the myocardial injury was assessed for each slice (Table 8). Native T1 mapping had the highest sensitivity in identifying myocardial injury from mid-ventricular slices (91.3% sensitivity and 100% specificity). Apical slices demonstrated the lowest sensitivity and specificity for identifying myocardial injury by T1 mapping (68.8% sensitivity and 50% specificity) (**Table 9).**

Table 9: Sensitivity, specificity, positive predictive values (PPV), and negative predictive values (NPV) of native T1 maps for identifying irreversible myocardial injury as defined by abnormally

high SI in LGE images, in apical, midventricular, basal slices, and all slices. Native T1 maps had the highest sensitivity in midventricular slices with 91.3% and 100% specificity.

Slices	Sensitivity	PPV	Specificity	NPV
Apex	68.8%	91.7%	50%	16.7%
Mid-ventricular	91.3%	100%	100%	50%
Base	85.7%	100%	100%	20%
Global	83.6%	98.2%	80%	26.7%

3.4.2. Accuracy values for LGE in identifying myocardial injury using T1 map as the ground truth technique

For this assessment, we considered T1 mapping colour-scale images as the ground truth technique and copied the contours from these images to the LGE images (Table 10).

The ability of LGE imaging in identifying myocardial injury as defined by abnormally high T1 is demonstrated in Table 10. The kappa coefficient value of agreement in the apical, basal, and mid-ventricular slices shows a good agreement (0.74, 0.67, and 0.63, respectively).

Table 10: Agreement between native T1 map (color- scale) and LGE images in identifying myocardial injury: Demonstrating the agreement in identifying injury in LGE images from T1 map. In all slices there was a substantial degree of agreement in identifying myocardial injury in LGE images from T1 map.

Identifying myocardial injury	**Apical**	**Mid-ventricular**	**Basal**
Measure of agreement from color T1 map to LGE images (kappa value)	**0.74**	**0.63**	**0.67**

3.5. Identifying the regional distribution of myocardial damage

The regional distribution of myocardial damage was assessed in all three slices of the LGE images and T1 maps. LGE images showed a similar fibrosis pattern between LGE and T1 maps in 24 (82.75%) of the 29 basal slices. The commonly observed patterns were: Transmural (18/24, 75%) transmural, subendocardial (15/24, 62.5%), RV insertion sites (4/24, 16.66%), septal mid-wall (2/24, 8.33%), and subepicardial (6/24, 25%).

In 5 basal slices with varying distribution patterns between LGE images and T1 maps, two slices (40%) slices had subepicardial, one slice (20%) had a transmural pattern, and one (20%) had a subendocardial distribution. Three (60%) T1 maps showed a diffuse pattern, while one (20%) LGE slice had a subepicardial pattern, and another LGE slice (20%) had a transmural pattern.

Twenty-two (88%) out of 25 mid-ventricular slices had the same fibrosis pattern in the T1 map and the LGE images: 13 (59%) were transmural, 9 (41%) subendocardial, 6 (27%) at an RV insertion, and 4 (18%) were subepicardial.

In three mid-ventricular slices where the injury did not show the same distribution pattern in T1 maps and LGE images, one (33%) was subendocardial and two were subepicardial. Two T1 maps had a transmural pattern.

Eleven out of 17 (65%) apical slices had the same fibrosis pattern in the T1 map as in LGE images, with seven (64%) being transmural, 4 (36%) subendocardial, and 3 (27%) at the RV insertion sites. In 6 (35%) apical slices where T1 maps and LGE images did not have the same distribution patterns for myocardial damage, 2 (33%) slices had a diffuse distribution pattern in LGE images, while in T1 maps, 3 (50%) apical slices had a diffuse distribution pattern. Four (67%) slices had a transmural distribution pattern in LGE images, while this was the case in only one (17%) of the T1 maps slice had a transmural pattern.

The accuracy of identifying the myocardial tissue damage distribution by T1 mapping was assessed using LGE images as the ground truth. The kappa value for the level of agreement was as follows: Apical: 0.697, mid-ventricular: 0.84, basal: 0.724 (**Table 11).**

Table 11: Agreement between regional distribution pattern of myocardial damage in the T1 map detected from LGE images. Demonstrating the agreement in the regional distribution pattern of tissue damage in the T1 map based on LGE images. Mid-ventricular slices have the highest agreement (kappa value= 0.840)

Distribution of myocardial damage	Apical	Mid-ventricular	Basal
Measure of agreement from LGE to T1 map (kappa value)	**0.697**	**0.840**	**0.724**

A segmental analysis was conducted based on the American Heart Association (AHA) heart segmentation to compare the segments with myocardial injury in T1 maps and LGE images. The agreement among the segments with myocardial injury in both LGE image and T1 maps was assessed by a McNemar test to identify the presence of the agreement between segments (**Table 12**). The McNemar test showed that there is not a significant disagreement between the LGE and T1 mapping images in identifying the myocardial injury (p values of 0.32, 0.41, and 0.56 for apical, midventricular, and basal slices, respectively).

Table 12*:* McNemar test of the agreement between segments with the presence of elevated T1 mapping value and enhancement in LGE. There is no significant difference between involved AHA segments in the T1 map and LGE images

Slice	McNemar value
Apex	0.32
Mid-ventricle	0.41
Base	0.56

3.6. Identifying the extent of myocardial damage

Figure 23 shows a box-and-whisker plot of the results for the extent of myocardial injury in T1 mapping and LGE images. Affected areas suggesting myocardial injury appeared larger in T1 maps than in the LGE images (**Figure 23).**

In the apical slices, the enhanced area identified in the LGE image had a median of 0.77 cm^2 and an interquartile range (IQR) of 0.69. The areas in apical T1 maps had a median of 1.26 cm^2 and IQR of 2.27. A Wilcoxon signed-rank test demonstrated that the area of myocardial injury in T1 maps was larger than the area of myocardial injury from the LGE images in apical slices (Z= -2.03, sig. (2-tailed) =0.021).

In the mid-ventricular slices, the abnormal myocardium identified in the LGE images had a median area of 1.58 cm^2 and IQR of 1.44. These areas in the T1 map in this slice had a median of 1.65 cm^2 and IQR of 2.0. A Wilcoxon signed-rank test confirmed that the areas of myocardial injury in the mid-ventricular T1 maps were larger than the abnormal area in the corresponding LGE images (Z= -3.28, sig (2-tailed) =.001).

In basal slices, the abnormal myocardium in the LGE image had a median area of 2.09 cm^2 with an IQR of 2.75. The area that the T1 map identified as a pathologic area had a median of 3.43 cm^2 with an IQR of 3.32. The Wilcoxon signed-rank test confirmed that the median area of the myocardial injury identified by the T1 map was larger than the LGE images in the basal slices (Z= -3.5, sig (2-tailed) =.000).

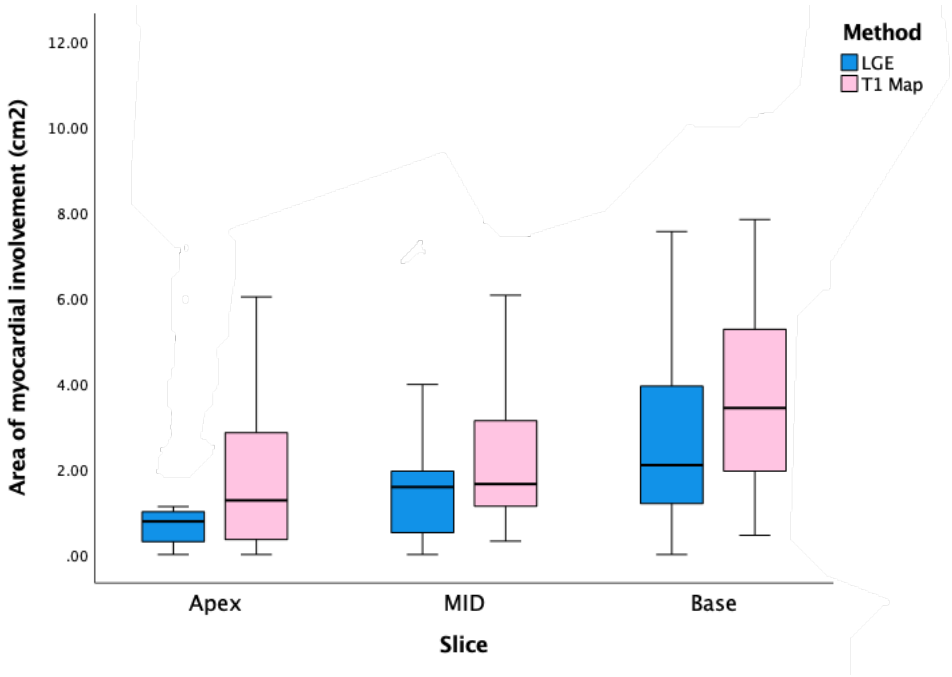

Figure 23: Area of myocardial injury identified by LGE and T1 map sequences: Box-and-whiskers plot of the area (cm^2) of abnormal myocardium in LGE images and in native T1 map in three slices (apex, mid-ventricular, and base), which appeared larger in native T1 map than in LGE; which was the case in all myocardial slices. (Wilcoxon signed-rank test values for apex= (Z= -2.03, p=.021), mid= (Z= -3.28, p=.001), and base= (Z= -3.5, p = .000).

In 18 apical slices, 13 (72.22 %) had a larger area of myocardial injury in T1 maps, while 3 patients (16.67 %) had a larger abnormal area in LGE images, and 2 patients (11.11 %) showed a similar size of myocardial injury. The largest difference between the identified area of myocardial injury from the LGE images and T1 mapping was 2.18 cm^2, with the T1 mapping identifying a larger area than the LGE images.

In 25 mid-ventricular slices, the area of myocardial injury was larger in T1 maps in 16 patients (64%), while the area was larger in LGE images in 5 patients (20%) and was similar in 4 patients (16%).

The largest difference between the identified area of myocardial injury from the LGE images and T1 mapping was 3.07 cm^2, with the T1 mapping identifying a larger area than the LGE images.

In 29 basal slices, 21 patients (72.41%) had a larger identified area of myocardial injury in T1 maps, while in 6 patients (20.68%), the area was larger in LGE images, and was similar in 2 patients (6.89%).

The largest difference between the identified area of myocardial injury from the LGE images and T1 mapping is 5.69 cm^2, with T1 mapping identifying a larger myocardial injury area than LGE images.

3.7. T2 mapping images analysis:

Based on the presence of an elevated T2, slices were dichotomized into groups of either acute (n=33) or chronic (n=25) myocardial events.

Of all slices, eight apical slices, 15 mid-ventricular slices, and ten basal slices have elevated T2 mapping values in the area where both the LGE image and T1 mapping images identified myocardial injury.

In chronic myocardial damage, the median ± IQR area of myocardial injury identified by the LGE images was 1.58± 2.48 and by the T1 map 1.02± 2.71, which were not significantly different (0.310).

In acute cases, the median ± IQR area of myocardial injury identified by LGE was 1.57± 1.69 and by the T1 map was 2.25± 2.3; $p<0.001$ for the difference). In patients with acute myocardial events, the area was larger in T1 maps than in LGE images **(Figure 24)**.

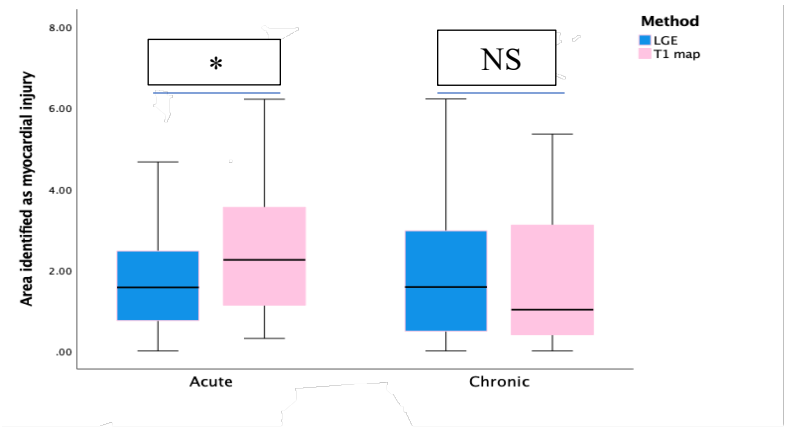

Figure 24: Areas of myocardial injury identified by T1 maps and LGE images in acute and chronic cases: In patients with acute myocardial injury, the abnormal area was significantly larger (*) in native T1 maps than in LGE images ($p<0.001$). In chronic cases, abnormal areas were similarly sized in native T1 maps and LGE images ($p = 0.301$). (*): significant difference; (NS): Difference statistically not significant.

In slices with an acute injury, the area identified as myocardial injury by the T2 map and LGE images is not significantly different from each other. However, the native T1 map identifies a larger area of myocardial injury in all slices from the LGE images and T2 map (**Figure 25).**

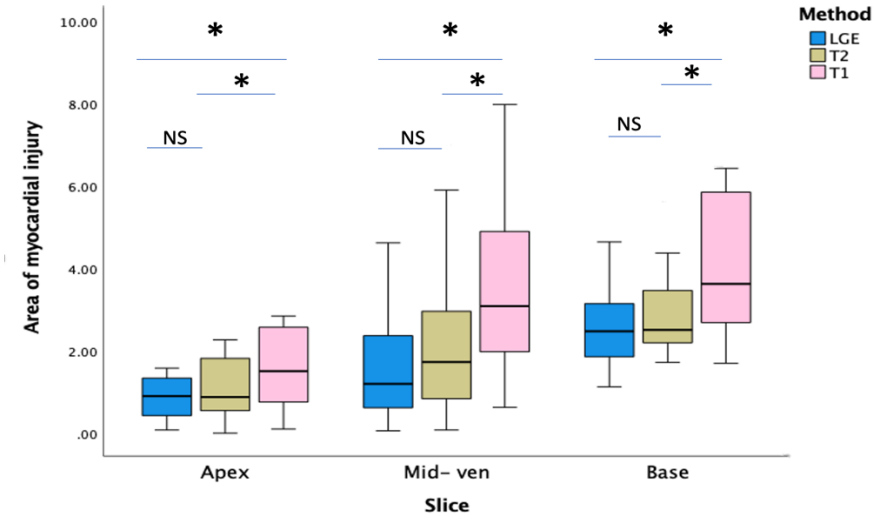

Figure 25: **The area of myocardial injury identified by native T1 and T2 maps and LGE images in acute cases:** Native T1 maps displayed a significantly larger area of myocardial injury in all slices compared to LGE images and T2 maps. In all slices, LGE images and T2 maps identified a similar area of myocardial injury. (*)statistically significantly different; (NS): No statistical difference.

3.6.1. Myocardial edema in T2 maps and LGE images

The Agreement between native T2 mapping and LGE imaging in identifying the area of myocardial injury is demonstrated in **Table 13.**

Table 13: Agreement between the location of myocardial injury in T2 maps and LGE images. Mid-ventricular slices had the best agreement (kappa value= 0.819

Identifying edema	Apical	Mid-ventricular slices	Basal
Measure of agreement from LGE to T2 map (kappa value)	0.681	0.819	0.647

Mid-ventricular slices showed an almost perfect agreement (kappa value= 0.819) in identifying the area of myocardial injury. Apical and basal slices had an agreement of 0.681 and 0.647, respectively.

3.7. Interclass correlation between two readers in identifying image analysis

Two different readers analyzed 21 randomly selected slices (from 9 patients) for repeatability analysis. The ICC based on a two-way random effect model on single ratings and absolute agreement between raters 1 and 2 is presented in **Table 14.**

Table 14: Inter-class correlation between two readers: ICC for the assessment of the area by the LGE images and native T1 map in 20 randomly selected slices.

Parameter	ICC	95% confidence interval
Area with LGE enhancement	0.937	0.651- 0.981
Area with elevated T1 in native T1 map	0.955	0.886- 0.982

The ICC for inter-rater repeatability of identifying the enhanced area in LGE was good (0.937), albeit with a statistical variance (0.651-0.981). The ICC for inter-rater repeatability for T1 mapping was high at 0.955 (0.886- 0.982) (**Table 14**).

The kappa value in measuring the degree of agreement between two readers regarding identifying the area with the elevated T1 values in the same anatomical area that the LGE images identified enhancement, was 0.885 (**Table 14**).

CHAPTER 4

4. DISCUSSION

This study examined the agreement between native mapping and LGE imaging in assessing myocardial injury in ischemic cardiomyopathy patients (ICMP). The focus was on identifying the presence and on measuring the extent of myocardial injury. The findings indicate that while T1 mapping can identify myocardial injury in the same location as LGE images, native T1 mapping may overestimate the area of myocardial damage. However, the combination of T1 and T2 mapping images could well differentiate between acute and chronic myocardial injury and had a very good agreement in identifying the extent of the myocardial injury area when compared to LGE images.

4.1. Identifying the presence of tissue damage

We compared the two methods, LGE imaging and mapping, interchanging both as the ground truth techniques in confirming and validating the area of myocardial injury by direct observation (154).

4.1.1. LGE images as the ground truth technique to identify myocardial injury

Due to the clinical importance of LGE in assessing ischemic myocardial injury, in the first part of the study, LGE was used as the ground truth technique to identify myocardial tissue damage for comparisons with T1 and T2 mapping images. LGE is known and utilized as the ground gold standard technique in evaluating ischemic fibrosis in the clinical setting (126) by providing valuable information about the location, extension, and pattern of myocardial injury (126).

Sometimes, LGE imaging is also used to quantify viable myocardium (viability) in the injured area, which plays role in clinical decision making to move to revascularization (8).

LGE imaging offers complete coverage of the left ventricle with eight to ten short axial slices, and three long axial slices, which helps in identifying a myocardial enhancement (cross-referencing approach) in different planes to confirm the presence and distribution pattern of enhancement. The complete left ventricular coverage allows measuring the percentage of the volume of myocardial tissue compared to the total myocardial mass as a measure of the scar burden. The scar burden is important in the prognosis assessment of the ICMP patients (132). Scar burden assessment by LGE CMR before major cardiac surgery, coronary artery bypass graft, had shown that smaller enhancement volumes were related to better survival after surgery (132). Complete coverage of the left ventricle with short and long-axis views therefore may be important in the assessment of the myocardial injury.

Typically, CMR mapping is performed in three slices, basal, mid-ventricular, and apical. For each slice, a breath-hold with a duration of 17 heartbeats is performed to 'freeze' the motion of the heart induced by breathing. The images are obtained at end-diastole. Because of these relatively long acquisition times, typically only three mapping slices are obtained (77). This work compared these three mapping slices to their corresponding slices from the LGE images with the same slice location and similar anatomical landmarks. T1 mapping images displayed an excellent agreement with LGE images in evaluating the presence and location of ischemic injury in midventricular and basal slices (**Table 8**). This finding implies that native T1 mapping has the potential to identify the

presence and location of ischemic myocardial damage in mid-ventricular and basal slices. No study had reported agreement between the slices from LGE imaging and mapping.

The tissue characterization information from one or two axial slices is not sufficient to make a clinical decision in an ischemic injury. In addition, there is no standard regarding the required number of slices for a quantitative assessment of the ischemic tissue damage; the minimal adequate number of slices for myocardial damage assessment depends on the pattern and timing of injury (158). A study has shown that a basal or mid-ventricular slice of the native T1 mapping can accurately identify the distribution of diffuse myocardial injury within an acquired slice (133). To rule out or rule in myocardial injury, full coverage of the ventricle would be advantageous.

Novel native mapping techniques such as MR Multitasking can indeed provide full coverage of the left ventricle without the need for breath-holding (134), or with shorter breath-holding time (MR Fingerprinting) (135). Shorter breath-holding periods are particularly useful in severely sick patients with shortness of breath or with problems following breathing instructions. These novel methods are currently being evaluated for their clinical feasibility and utility, thus still considered a research tool; however, they have the potential to increase the precision of myocardial tissue characterization (121) while also providing quantitative information on LV function (33).

4.1.1.1 Sensitivity and specificity of T1 mapping in ischemic myocardial injury using LGE imaging as the ground truth technique

This work demonstrated that native T1 mapping had high sensitivity and specificity of 83.6% and 80%, respectively, to identify fibrosis in the T1 map, using LGE as the standard of truth. In mid-ventricular slices, the sensitivity and specificity were 91.3% and 100%, respectively, while in basal

slices, the observed sensitivity was 85.7%, with a specificity of 100%. This is consistent with published work that demonstrated a 96% sensitivity and 91% specificity of native T1 mapping in identifying myocardial fibrosis in acute myocardial infarction (98). In an animal study, T1 mapping had a sensitivity of 75.6% and specificity of 96.3% to detect myocardial infarction by histopathology (110). Our results, albeit limited by small sample size, therefore underscore the potential of T1 mapping for correctly identifying the area of myocardial injury.

4.1.1.2. Myocardial injury distribution pattern in T1 mapping applying LGE images pattern as the ground truth technique

We demonstrated that the T1 mapping could assess the distribution of fibrosis patterns with a strong agreement with LGE findings in co-located mid-ventricular slices (kappa: apical= 0.7, mid-ventricular= 0.84, basal= 0.72). Based on this result, native T1 mapping has the potential to be used in midventricular slices to assess the distribution of fibrosis with a strong agreement from LGE images. However, this finding was observed in only one slice, which does not apply to the other slices.

4.1.2. T1 maps as the ground truth imaging technique to identify myocardial injury

In the second analysis, T1 maps were used as the reference to identify the myocardial injury. We found that the degree of agreement between the T1 map colour scale and LGE images for all slices was substantial (kappa values for apical: 0.74, mid-ventricular: 0.63, and basal: 0.67) (**Table 10).**

4.2 Differences in the agreement between LGE and T1 mapping as the reference:

This study applied LGE imaging or T1 mapping as the ground truth imaging method to identify the myocardial injury, the application of these imaging methods provided different agreement values. One reason that explains the different kappa values in identifying the myocardial injury that may occur is because of the different image analysis approaches applied in each method. In the analysis of LGE images, we applied the 5SD method to compare the signal intensities of the normal myocardium to the injured myocardium. Using an intraindividual reference may be associated with less variability induced by confounders such as sex, or heart rate. In the analysis of the colour scale T1 mapping images, the pathologic values for myocardial injury are defined based on the normal global mean and standard deviation of mapping values of the healthy volunteers for the specific scanner and mapping sequence (89). The 2SD threshold is defined as the cut-off value, for which values greater than 2SD above or below the mean are defined as pathologic (89). Native mapping does not require a region in the myocardium as normal reference tissue, which makes mapping a less reader-dependent approach and less challenging in the assessment of myocardial injuries (89).

Another factor may be the selection of the healthy volunteers to define the normal mapping values. The enrolment of healthy volunteers in the studies is based on their self-reported health status, but of course, this selection may introduce bias and variability that ultimately affects the defined normal values and their accuracy or utility (102). Rigorous inclusion and exclusion criteria for recruiting a healthy volunteer population for each scanner and mapping sequences can help to decrease this overlap. Such risk for bias can be reduced by a complete physical exam, family history, or electrocardiogram (ECG) before enrolling participants as healthy volunteers in a study

(136). Another option to rule out participants with myocardial abnormalities as healthy participants would have been to inject gadolinium to confirm the absence of myocardial fibrosis. This study is not based on the gadolinium application in the healthy participants to identify the healthiest participants for mapping values establishment which can be one limitation of the study.

The observed difference in agreements between slices (kappa values LGE as the ground truth: apical= 0.66, mid-ventricular= 0.93, basal= 0.87) can be explained by anatomical aspects and wall thickness in these slices. In basal slices, the left-ventricular outflow tract, where the aortic root leaves the heart (137). In apical slices, the partial volume effect can impair image analysis and lead to errors in the interpretation of the result (125).

4.3. Extension of myocardial injury

This study demonstrated differences between T1 mapping and LGE in assessing the presence and extent of myocardial injury. Areas with myocardial injury appeared larger when quantified by T1 mapping as compared with LGE. These results correspond with a previous study (138). The extension of fibrosis identified by LGE is a valuable risk stratification tool in assessing the occurrence of ventricular dysrhythmia in fibrotic myocardial tissue (46).

Fibrosis extension helps in clinical decision-making and management of the patient to prevent the event from reoccurrence (46). As electrophysiology studies have shown, myocardial scar as visualized by LGE is associated with ventricular arrhythmia and sudden cardiac death (SCD) in patients (139). SCD can be prevented by an appropriate insertion of an implantable-cardioverter defibrillator (ICD) in patients at an elevated risk. LGE-CMR therefore can help stratify patients for

ICD implantation (46). A validation study on mapping to assess the outcome and management of this population can be helpful in mapping roles in the clinical setting.

Based on our findings, native T1 mapping with a 2SD threshold may overestimate the extension of the area identified as myocardial injury in ICMP. This of course depends on the selection of cut-off/threshold values (140). We selected a cut-off of 2SD above to mean normal values in accordance with the recommendations of the Society for Cardiovascular Magnetic Resonance. Previous studies using T1 mapping in animals (110) and humans (98) applied cut-off values of more than 3SD above normal to identify irreversible ischemic injury.

The overestimation of the area identified as myocardial injury by T1 mapping can also be explained by the presence of myocardial edema. Myocardial T1 is increased in the presence of myocardial edema and the resulting increase of free water. T1 mapping has high diagnostic accuracy in identifying edema compared to other CMR edema imaging methods such as Short Tau Inversion Recovery (STIR) T2-weighted CMR (141). In acute myocardial ischemic events, we expect edema in the area at risk (AAR), i.e., the area that is not infarcted yet but had been exposed to significant transient ischemia (142) (153). LGE only identifies fibrosis or, in the acute stage of myocardial infarction, necrosis, while the T1 mapping can identify fibrosis and edema. Since the latter often surrounds the necrotic area, T1 is likely to show a larger affected area than LGE, which is only moderately sensitive to edema. In our results, the overestimation of myocardial injury by T1 maps was mostly present in the setting of an acute injury, where the concurrent elevation of T2 mapping values indicated edema in that region (**Figure 24).**

Our findings suggest that the 2SD threshold in T1 maps can identify the area of myocardial injury, both fibrosis, and edema, while LGE visualized irreversible injury only. Previous work has shown that in patients with non-ischemic dilated cardiomyopathy, native T1 mapping can detect myocardial changes sooner than LGE (105). In a study in dilated cardiomyopathy patients, T1 was increased also in areas with normal LGE appearance. This underscores the role of T1 mapping in assessing diffuse fibrosis, where LGE imaging is unsuccessful to identify fibrosis (107). It remains unclear whether native T1 mapping may be able to identify myocardial injury earlier than LGE; Prospective, longitudinal studies may be needed to identify better the role of mapping in myocardial injury assessment from the early stage of the ischemic event to their later stage.

It may be possible finding the best threshold in mapping or LGE imaging for correctly identifying the extent of myocardial injury through Machine Learning (ML) algorithms (143). As part of artificial intelligence, ML can extract data based on a specific parameter defined beforehand, such as contrast, noise, texture, and motion (143). After training the algorithm in a large data set (168), machine learning algorithms can be used to measure variables (143).

No patients in the current study had an area of hemorrhage in the core infarct, however, this may be present in up to 25 % of patients with ICMP, particularly the ones that experience reperfusion (144). Myocardial hemorrhage can be identified by low signal intensities inside the infarcted area, caused by degradation products of hemoglobin and methemoglobin (144). The clinical importance of this population is that this hemorrhagic area in the ischemic event is associated with large infarct size, no improvement of cardiac contractile ability over time, increased LV end-systolic volume, revascularization, and poor prognosis (145). This population

can be studied in the future to understand the impact of the hemorrhagic injury on the LGE imaging and T1 mapping.

4.4. Moving toward a non-contrast imaging technique

The recent consensus of the American College of Radiology and the National Kidney Foundation on the use of macrocyclic gadolinium application emphasized the safety of gadolinium-based contrast agents in imaging even in a patient with GFR <30 or acute kidney injury. The gadolinium standard dose is 0.1 mmol/kg, which has a low risk (zero events among 4931 administrated cases) of nephrogenic systemic fibrosis (147). This consensus addressed the risks associated with gadolinium-based contrast agents in patients with significant renal impairment (146) and made its clinical application more common.

As explained, gadolinium is a well-tolerated and safe contrast medium in imaging; however, its application is time-consuming because it requires the insertion of the IV catheter for administration and requires at least 10 minutes of waiting time to perform LGE imaging to visualize the scar. Additionally, local expertise is required as MRI technicians are trained to select an appropriate inversion time to create the maximum contrast between blood and the myocardium on the LGE images. This makes gadolinium imaging also a subjective approach in both phases of image acquisition and image analysis.

When assessing LGE images, the clinician visually identifies the presence or absence of enhancement. In images with suboptimal image quality or artifacts, such reading is dependent on the expertise and experience of the reader, which is a significant limitation of this method, in

addition to the need for an individual determination of the sequence parameter inversion time, and the associated cost and time needed for contrast injection.

For native T1 and T2 mapping image acquisition, there is no need to select manually a nulling inversion time or wait 10 minutes to visualize the injured tissue. The fewer time patients spend in the scanner, the more comfortable the imaging experience is for them. The time saved by using native CMR mapping instead may allow for an increase in CMR accessibility for patients.

The agreement between the native mapping and LGE imaging supports moving toward a CMR imaging approach without IV catheter insertion and waiting time for gadolinium to visualize the injury.

T1 and T2 mapping, as confirmed in our study, can provide valuable information regarding the timing, presence, distribution, and extension of the injury (148). Incorporating other non-contrast techniques such as cine and strain in a large population of ICMP can help validate a non-contrast approach in the clinical assessment of these patients.

One accepted application of CMR is assessing wall motion from cine images. Within seconds after the onset of no-flow ischemia, the cascade of various cellular changes such as sarcomere dysfunction leads to a loss in wall motion. In mild injury, the wall becomes hypokinetic (149), while in more severe injury, akinesia or dyskinesia may be induced. If revascularization occurs early after the ischemic injury, the wall motion abnormality can be reversible (149). However, if the ischemic injury takes long or is repeated, dysfunction may become irreversible (149). The

clinical evaluation of the wall motion abnormality is visually based on the presence or absence of the impairment.

ICMP not only affects wall motion but also myocardial wall thickness. In chronic ischemic cardiomyopathy, the affected wall typically appears thinned (150). This decrease in wall thickness happens because of the death of the cardiac cells and fibrosis formation, followed by the scar shrinkage as a part of the healing process (150). Wall thickness, therefore, has been used for many years to assess myocardial viability for selecting the patients for revascularization (150). Values of less than 5.5 mm have been used to define non-viable myocardium (150). Quantitative information on wall motion abnormality and wall thickness can be extracted from cine images which are part of most CMR protocols and provide volumetric heart data. Adding wall motion and wall thickness to mapping may lead to an even higher diagnostic accuracy.

4.5. Potential limitations

This study has several limitations. This work was a retrospective study with small sample size and a limited number of matching slices per patient available for the analysis.

Female participants included only 9% of the total participants in this study while cardiovascular disease is a leading cause of death in this population (155). The clinical utility of CMR has been endorsed by the society of cardiovascular magnetic resonance imaging since there is no radiation involved which can potentially lead to breast cancer (156). Additionally, CMR has been recommended as a diagnostic tool for identifying myocardial injury in myocardial infarction with no obstructive coronary arteries (less than 50% stenosis), which occurs mostly in younger women (157).

Future prospective studies with a larger population and including more female participants may provide more insight into the role of native T1 and T2 mapping in the assessment of ischemic myocardial injury to move toward a free contrast CMR technique (151).

For image analysis, placing the ROI in the normal myocardium and segmentation was done manually, which may introduce human error by the reader and affect the result of the study. Automatic image analysis and segmentation methods for mapping and LGE images may reduce the chance of error caused by the bias that readers bring to the study. Although there could be a bias in these aspects, the excellent inter-observer agreement (high ICC) makes this unlikely.

4.6. Future directions of native mapping CMR

Longitudinal studies in patients with ischemic cardiomyopathy are warranted to assess the myocardial changes at the start of the ischemic (acute phase) event and later (6 months or more after the injury) (chronic phase) by tissue characterization techniques (LGE imaging and mapping) and assess the patients' prognosis and outcome in all-cause mortality and hospitalization.

The role of several confounders should be assessed, such as microvascular changes due to ischemia, hemorrhagic ischemic injury, and reperfusion injury as a part of the ischemic cardiomyopathy spectrum to verify mapping changes. Eventually, the utility of mapping as a part of diagnostic decision-making should be investigated, especially the impact of its clinical application on patient outcomes.

Native mapping as a part of CMR imaging can identify myocardial injury (edema, necrosis, scar, fibrosis). Adding other non-contrast imaging parameters, e.g., markers of function such as strain may allow for short, efficient protocols.

4.6. Conclusion

Our results indicate a good agreement between T1 mapping and LGE to identify and quantify the extent of myocardial injury in the ICMP patient population. However, T1 mapping overestimates the area of myocardial injury if defined by LGE. This may be due to the sensitivity of T1 maps to the presence of myocardial edema.

Prospective clinical studies in this patient population are now warranted to clarify the role of native mapping compared to LGE imaging in assessing the ischemic myocardial injury, as native techniques would come with significant advantages concerning patient safety and comfort, as well as logistics, and cost.

5.REFERENCES

1.Lloyd-Jones, D., Adams, R., Brown, T., Carnethon, M., Dai, S., & De Simone, G. et al. (2010). Heart Disease and Stroke Statistics—2010 Update. *Circulation*, *121*(7). doi: 10.1161/circulationaha.109.192667

2.Gaziano, T. A., Bitton, A., Anand, S., Abrahams-Gessel, S., & Murphy, A. (2010). Growing epidemic of coronary heart disease in low-and middle-income countries. *Current problems in cardiology*, *35*(2), 72-115.

3.McCrohon, J. A., Moon, J. C. C., Prasad, S. K., McKenna, W. J., Lorenz, C. H., Coats, A. J. S., & Pennell, D. J. (2003). Differentiation of heart failure related to dilated cardiomyopathy and coronary artery disease using gadolinium-enhanced cardiovascular magnetic resonance. *Circulation*, *108*(1), 54-59

4.Bhandari, B., Rodriguez, B. S. Q., & Masood, W. (2020). Ischemic Cardiomyopathy. *StatPearls [Internet]*.

5.Sanchis-Gomar, F., Perez-Quilis, C., Leischik, R., & Lucia, A. (2016). Epidemiology of coronary heart disease and acute coronary syndrome. *Annals of translational medicine*, *4*(13).

6.Kramer, C. M. (2006). The expanding prognostic role of late gadolinium enhanced cardiac magnetic resonance. *Journal of the American College of Cardiology*, *48*(10), 1986-1987

7.Omeh, D. J., & Shlofmitz, E. (2020). Angiography. StatPearls [https://www.ncbi.nlm.nih.gov/books/NBK557477/

8.Neumann, F. J., Sousa-Uva, M., Ahlsson, A., Alfonso, F., Banning, A. P., Benedetto, U., ... & Zembala, M. O. (2019). 2018 ESC/EACTS Guidelines on myocardial revascularization. *European heart journal*, *40*(2), 87-165

9.Rajiah, P., Desai, M. Y., Kwon, D., & Flamm, S. D. (2013). MR imaging of myocardial infarction. *Radiographics*, *33*(5), 1383-1412.

10.Wu, H. D., & Kwong, R. Y. (2008). Cardiac magnetic resonance imaging in patients with coronary disease. *Current treatment options in cardiovascular medicine*, *10*(1), 83–92. https://doi.org/10.1007/s11936-008-0009-x

11.Pasotti, M., Prati, F., & Arbustini, E. (2006). The pathology of myocardial infarction in the pre- and post-interventional era. *Heart (British Cardiac Society)*, *92*(11), 1552–1556. https://doi.org/10.1136/hrt.2005.086934

12.Frangogiannis N. G. (2014). The inflammatory response in myocardial injury, repair, and remodelling. *Nature reviews. Cardiology*, *11*(5), 255–265. https://doi.org/10.1038/nrcardio.2014.28

13. Bassett, E. G., & Wakefield, J. S. J. (2008). Elastic fibers in myocardial scars in rats: development teraction with other components. *Connective tissue research*, *49*(5), 321-327

14.De Jong, S., van Veen, T. A., van Rijen, H. V., & de Bakker, J. M. (2011). Fibrosis and cardiac arrhythmias. *Journal of cardiovascular pharmacology*, *57*(6), 630-638

15.Germain, P., El Ghannudi, S., Jeung, M. Y., Ohlmann, P., Epailly, E., Roy, C., & Gangi, A. (2014). Native T1 mapping of the heart - a pictorial review. *Clinical Medicine Insights. Cardiology*, *8*(Suppl 4), 1–11. https://doi.org/10.4137/CMC.S19005

16.Tahir, E., Sinn, M., Bohnen, S., Avanesov, M., Säring, D., Stehning, C., ... & Lund, G. K. (2017). Acute versus chronic myocardial infarction: diagnostic accuracy of quantitative native T1 and T2 mapping versus assessment of edema on standard T2-weighted cardiovascular MR images for differentiation. *Radiology*, *285*(1), 83-91

17.Kim, H. W., Farzaneh-Far, A., & Kim, R. J. (2009). Cardiovascular magnetic resonance in patients with myocardial infarction: current and emerging applications. *Journal of the American College of Cardiology*, *55*(1), 1-16

18.Barclay, J. L., Egred, M., Kruszewski, K., Nandakumar, R., Norton, M. Y., Stirrat, C., ... & Hillis, G. S. (2007). The relationship between transmural extent of infarction on contrast enhanced magnetic resonance imaging and recovery of contractile function in patients with first myocardial infarction treated with thrombolysis. *Cardiology*, *108*(4), 217-222

19.Choi, K. M., Kim, R. J., Gubernikoff, G., Vargas, J. D., Parker, M., & Judd, R. M. (2001). Transmural extent of acute myocardial infarction predicts long-term improvement in contractile function. *Circulation*, *104*(10), 1101-1107)

20.Sprawls, P. (1993). *Physical principles of medical imaging*. Gaithersburg: Aspen Publishers. Chapter 3

21.Berger A. (2002). Magnetic resonance imaging. *BMJ (Clinical research ed.)*, *324*(7328), 35. https://doi.org/10.1136/bmj.324.7328.35

22.Ridgway, J. P. (2010). Cardiovascular magnetic resonance physics for clinicians: part I. *Journal of cardiovascular magnetic resonance*, *12*(1), 1-28

23.Berger A. (2002). Magnetic resonance imaging. *BMJ (Clinical research ed.)*, *324*(7328), 35. https://doi.org/10.1136/bmj.324.7328.35

24. Kramer, C. M. (2006). The expanding prognostic role of late gadolinium enhanced cardiac magnetic resonance. *Journal of the American College of Cardiology*, *48*(10), 1986-1987

25. Sprawls, P. (1993). *Physical principles of medical imaging*. Gaithersburg: Aspen Publishers. Chapter 3.

26. Gallagher, T. A., Nemeth, A. J., & Hacein-Bey, L. (2008). An introduction to the Fourier transform: relationship to MRI. *American journal of roentgenology*, *190*(5), 1396-1405

27.Nacif, M. S., Zavodni, A., Kawel, N., Choi, E. Y., Lima, J. A., & Bluemke, D. A. (2012). Cardiac magnetic resonance imaging and its electrocardiographs (ECG): tips and tricks. *The international journal of cardiovascular imaging*, *28*(6), 1465–1475. https://doi.org/10.1007/s10554-011-9957-4

28.Tseng, W. Y. I., Su, M. Y. M., & Tseng, Y. H. E. (2016). Introduction to cardiovascular magnetic resonance: technical principles and clinical applications. *Acta Cardiologica Sinica*, *32*(2), 129

29.Look, D. C., & Locker, D. R. (1970). Time saving in measurement of NMR and EPR relaxation times. *Review of Scientific Instruments*, *41*(2), 250-251

30.Xiao, Y. D., Paudel, R., Liu, J., Ma, C., Zhang, Z. S., & Zhou, S. K. (2016). MRI contrast agents: Classification and application. *International journal of molecular medicine*, *38*(5), 1319-1326

31.Kim, R. J., Wu, E., Rafael, A., Chen, E. L., Parker, M. A., Simonetti, O., ... & Judd, R. M. (2000). The use of contrast-enhanced magnetic resonance imaging to identify reversible myocardial dysfunction. *New England Journal of Medicine*, *343*(20), 1445-1453

32.Klein, C., Schmal, T. R., Nekolla, S. G., Schnackenburg, B., Fleck, E., & Nagel, E. (2007). Mechanism of late gadolinium enhancement in patients with acute myocardial infarction. *Journal of cardiovascular magnetic resonance*, *9*(4), 653-658

33.Kim, H. W., Farzaneh-Far, A., & Kim, R. J. (2009). Cardiovascular magnetic resonance in patients with myocardial infarction: current and emerging applications. *Journal of the American College of Cardiology*, *55*(1), 1-16

34.Doltra, A., Hoyem Amundsen, B., Gebker, R., Fleck, E., & Kelle, S. (2013). Emerging concepts for myocardial late gadolinium enhancement MRI. *Current cardiology reviews*, *9*(3), 185-190

35.Kramer, C. M., Barkhausen, J., Bucciarelli-Ducci, C., Flamm, S. D., Kim, R. J., & Nagel, E. (2020). Standardized cardiovascular magnetic resonance imaging (CMR) protocols: 2020 update. *Journal of Cardiovascular Magnetic Resonance*, *22*(1), 1-18.

36. Holtackers, R. J., Van De Heyning, C. M., Nazir, M. S., Rashid, I., Ntalas, I., Rahman, H., ... & Chiribiri, A. (2019). Clinical value of dark-blood late gadolinium enhancement cardiovascular magnetic resonance without additional magnetization preparation. *Journal of Cardiovascular Magnetic Resonance*, *21*(1), 1-11

37.Flett, A. S., Hasleton, J., Cook, C., Hausenloy, D., Quarta, G., Ariti, C., ... & Moon, J. C. (2011). Evaluation of techniques for the quantification of myocardial scar of differing etiology using cardiac magnetic resonance. *JACC: cardiovascular imaging*, *4*(2), 150-156

38.Kim, R. J., Fieno, D. S., Parrish, T. B., Harris, K., Chen, E. L., Simonetti, O., ... & Judd, R. M. (1999). Relationship of MRI delayed contrast enhancement to irreversible injury, infarct age, and contractile function. *Circulation*, *100*(19), 1992-2002

39.Bondarenko, O., Beek, A. M., Hofman, M. B., Kühl, H. P., Twisk, J. W., Van Dockum, W. G., ... & Van Rossum, A. C. (2005). Standardizing the definition of hyperenhancement in the quantitative assessment

of infarct size and myocardial viability using delayed contrast-enhanced CMR. *Journal of Cardiovascular Magnetic Resonance*, *7*(2), 481-485.)

40.Alkhalil, M., Borlotti, A., De Maria, G. L., Wolfrum, M., Dawkins, S., Fahrni, G., ... & Choudhury, R. P. (2020). Hyper-acute cardiovascular magnetic resonance T1 mapping predicts infarct characteristics in patients with ST elevation myocardial infarction. *Journal of Cardiovascular Magnetic Resonance*, *22*(1), 1-12.

41.Eitel I, de Waha S, Wöhrle J, Fuernau G, Lurz P, Pauschinger M, et al. Comprehensive Prognosis Assessment by CMR Imaging After ST-Segment Elevation Myocardial Infarction. J Am Coll Cardiol. [Internet]. 2014;64:1217–26. Available from: http://linkinghub.elsevier.com/retrieve/pii/S0735109714056241

42. Eitel I, Desch S, Fuernau G, Hildebrand L, Gutberlet M, Schuler G, et al. Prognostic Significance and Determinants of Myocardial Salvage Assessed by Cardiovascular Magnetic Resonance in Acute Reperfused Myocardial Infarction. J Am Coll Cardiol. 2010;55:2470–9.

43.Schulz-Menger, J., Bluemke, D. A., Bremerich, J., Flamm, S. D., Fogel, M. A., Friedrich, M. G., ... & Nagel, E. (2013). Standardized image interpretation and post processing in cardiovascular magnetic resonance: Society for Cardiovascular Magnetic Resonance (SCMR) board of trustees task force on standardized post processing. *Journal of Cardiovascular Magnetic Resonance*, *15*(1), 1-19

44.Kellman, P., Arai, A. E., McVeigh, E. R., & Aletras, A. H. (2002). Phase-sensitive inversion recovery for detecting myocardial infarction using gadolinium-delayed hyperenhancement. *Magnetic Resonance in Medicine: An Official Journal of the International Society for Magnetic Resonance in Medicine*, *47*(2), 372-383

45.Hundley, W. G., Bluemke, D., Bogaert, J. G., Friedrich, M. G., Higgins, C. B., Lawson, M. A., ... & Neubauer, S. (2009). Society for Cardiovascular Magnetic Resonance guidelines for reporting cardiovascular magnetic resonance examinations. *Journal of Cardiovascular Magnetic Resonance*, *11*(1), 1-11

46.Scott, P. A., Rosengarten, J. A., Murday, D. C., Peebles, C. R., Harden, S. P., Curzen, N. P., & Morgan, J. M. (2013). Left ventricular scar burden specifies the potential for ventricular arrhythmogenesis: an LGE-CMR study. *Journal of cardiovascular electrophysiology*, *24*(4), 430–436. https://doi.org/10.1111/jce.12035

47.Seferović, P. M., Polovina, M., Bauersachs, J., Arad, M., Gal, T. B., Lund, L. H., ... & Filippatos, G. S. (2019). Heart failure in cardiomyopathies: a position paper from the Heart Failure Association of the European Society of Cardiology. *European journal of heart failure*, *21*(5), 553-576

48.Arai, A. E. (2008). Myocardial infarction and viability with an emphasis on imaging delayed enhancement. In *Cardiovascular magnetic resonance imaging* (pp. 351-375). Humana Press

49.Vöhringer, M., Mahrholdt, H., Yilmaz, A., & Sechtem, U. (2007). Significance of late gadolinium enhancement in cardiovascular magnetic resonance imaging (CMR). *Herz Kardiovaskuläre Erkrankungen*, *32*(2), 129-137

50. Reimer, K. A., & Jennings, R. B. (1979). The changing anatomic reference base of evolving myocardial infarction. Underestimation of myocardial collateral blood flow and overestimation of experimental anatomic infarct size due to tissue edema, hemorrhage, and acute inflammation. *Circulation*, *60*(4), 866-876

51.Wagner, A., Mahrholdt, H., Holly, T. A., Elliott, M. D., Regenfus, M., Parker, M., ... & Judd, R. M. (2003). Contrast-enhanced MRI and routine single photon emission computed tomography (SPECT) perfusion imaging for detection of subendocardial myocardial infarcts: an imaging study. *The Lancet*, *361*(9355), 374-379

52.Amado, L. C., Gerber, B. L., Gupta, S. N., Rettmann, D. W., Szarf, G., Schock, R., ... & Lima, J. A. (2004). Accurate and objective infarct sizing by contrast-enhanced magnetic resonance imaging in a canine myocardial infarction model. *Journal of the American College of Cardiology*, *44*(12), 2383-2389

53.Hammer-Hansen, S., Bandettini, W. P., Hsu, L. Y., Leung, S. W., Shanbhag, S., Mancini, C., ... & Arai, A. E. (2015). Mechanisms for overestimating acute myocardial infarct size with gadolinium-enhanced cardiovascular magnetic resonance imaging in humans: a quantitative and kinetic study. *European Heart Journal-Cardiovascular Imaging*, *17*(1), 76-84.

54. Arai, A. E. (2011). The cardiac magnetic resonance (CMR) approach to assessing myocardial viability. *Journal of Nuclear Cardiology*, *18*(6), 1095-1102

55. Kim, R. J., Wu, E., Rafael, A., Chen, E. L., Parker, M. A., Simonetti, O., ... & Judd, R. M. (2000). The use of contrast-enhanced magnetic resonance imaging to identify reversible myocardial dysfunction. *New England Journal of Medicine*, *343*(20), 1445-1453

56. Bello, D., Fieno, D. S., Kim, R. J., Pereles, F. S., Passman, R., Song, G., ... & Goldberger, J. J. (2005). Infarct morphology identifies patients with substrate for sustained ventricular tachycardia. *Journal of the American College of Cardiology*, *45*(7), 1104-1108

57. Nicod, P. E. H. R. A. A., Gilpin, E., Dittrich, H., Polikar, R., Hjalmarson, A., Blacky, A. R., ... & Ross Jr, J. (1989). Short-and long-term clinical outcome after Q wave and non-Q wave myocardial infarction in a large patient population. *Circulation*, *79*(3), 528-536.

58. Hutter Jr, A. M., DeSanctis, R. W., Flynn, T., & Yeatman, L. A. (1981). Nontransmural myocardial infarction: a comparison of hospital and late clinical course of patients with that of matched patients with transmural anterior and transmural inferior myocardial infarction. *The American journal of cardiology*, *48*(4), 595-602.

59. Marmor, A., Sobel, B. E., & Roberts, R. (1981). Factors presaging early recurrent myocardial infarction ("extension"). *The American journal of cardiology*, *48*(4), 603-610

60. Kwong, R. Y., Chan, A. K., Brown, K. A., Chan, C. W., Reynolds, H. G., Tsang, S., & Davis, R. B. (2006). Impact of unrecognized myocardial scar detected by cardiac magnetic resonance imaging on event-free survival in patients presenting with signs or symptoms of coronary artery disease. *Circulation*, *113*(23), 2733-2743

61. Kwong, R. Y., Sattar, H., Wu, H., Vorobiof, G., Gandla, V., Steel, K., ... & Brown, K. A. (2008). Incidence and prognostic implication of unrecognized myocardial scar characterized by cardiac magnetic resonance in diabetic patients without clinical evidence of myocardial infarction. *Circulation*, *118*(10), 1011-1020

62.Menacho, K., Ramirez, S., Segura, P., Nordin, S., Abdel-Gadir, A., Illatopa, V., ... & Moon, J. C. (2018). INCA (Peru) study: impact of non-invasive cardiac magnetic resonance assessment in the developing world. *Journal of the American Heart Association*, *7*(17), e008981

63.Ibrahim, E. S. H., Frank, L., Baruah, D., Rubenstein, J., Arpinar, V. E., Nencka, A., ... & Bergom, C. (2020). Value CMR: Towards a Comprehensive, Rapid, Cost-Effective Cardiovascular Magnetic Resonance Imaging. *medRxiv*

64.Jablonowski, R., Engblom, H., Kanski, M., Nordlund, D., Koul, S., van der Pals, J., ... & Arheden, H. (2015). Contrast-enhanced CMR overestimates early myocardial infarct size: mechanistic insights using ECV measurements on day 1 and day 7. *JACC: Cardiovascular Imaging*, *8*(12), 1379-1389.

65.Karamitsos, T. D., Piechnik, S. K., Banypersad, S. M., Fontana, M., Ntusi, N. B., Ferreira, V. M., ... & Neubauer, S. (2013). Noncontrast T1 mapping for the diagnosis of cardiac amyloidosis. *JACC: Cardiovascular Imaging*, *6*(4), 488-497

66.Kellman, P., Arai, A. E., McVeigh, E. R., & Aletras, A. H. (2002). Phase-sensitive inversion recovery for detecting myocardial infarction using gadolinium-delayed hyperenhancement. *Magnetic Resonance in Medicine: An Official Journal of the International Society for Magnetic Resonance in Medicine*, *47*(2), 372-383

67.Dass, S., Suttie, J. J., Piechnik, S. K., Ferreira, V. M., Holloway, C. J., Banerjee, R., ... & Watkins, H. (2012). Myocardial tissue characterization using magnetic resonance noncontrast t1 mapping in hypertrophic and dilated cardiomyopathy. *Circulation: Cardiovascular Imaging*, *5*(6), 726-733

68.Reiter, T., Ritter, O., Prince, M. R., Nordbeck, P., Wanner, C., Nagel, E., & Bauer, W. R. (2012). Minimizing risk of nephrogenic systemic fibrosis in cardiovascular magnetic resonance. *Journal of cardiovascular magnetic resonance : official journal of the Society for Cardiovascular Magnetic Resonance*, *14*(1), 31. https://doi.org/10.1186/1532-429X-14-31

69.Weinreb, J. C., Rodby, R. A., Yee, J., Wang, C. L., Fine, D., McDonald, R. J., ... & Davenport, M. S. (2020). Use of Intravenous Gadolinium-based Contrast Media in Patients with Kidney Disease: Consensus Statements from the American College of Radiology and the National Kidney Foundation. *Kidney Medicine*

70.O h-Ici, D., Jeuthe, S., Al-Wakeel, N., Berger, F., Kuehne, T., Kozerke, S., & Messroghli, D. R. (2014). T1 mapping in ischaemic heart disease. *European Heart Journal–Cardiovascular Imaging*, *15*(6), 597-602.

71.Gulani, V., Calamante, F., Shellock, F. G., Kanal, E., & Reeder, S. B. (2017). Gadolinium deposition in the brain: summary of evidence and recommendations. *The Lancet Neurology*, *16*(7), 564-570

72.Kramer, C. M., Barkhausen, J., Bucciarelli-Ducci, C., Flamm, S. D., Kim, R. J., & Nagel, E. (2020). Standardized cardiovascular magnetic resonance imaging (CMR) protocols: 2020 update. *Journal of Cardiovascular Magnetic Resonance*, *22*(1), 1-18

73.Taylor, A. J., Salerno, M., Dharmakumar, R., & Jerosch-Herold, M. (2016). T1 mapping: basic techniques and clinical applications. *JACC: Cardiovascular Imaging*, *9*(1), 67-81

74.Fung, B. M. (1986). [10] Nuclear magnetic resonance study of water interactions with proteins, biomolecules, membranes, and tissues. In *Methods in enzymology* (Vol. 127, pp. 151-161). Academic Press.

75.Kellman, P., & Hansen, M. S. (2014). T1-mapping in the heart: accuracy and precision. *Journal of cardiovascular magnetic resonance*, *16*(1), 2

76.Higgins, D. M., & Moon, J. C. (2014). Review of T1 mapping methods: comparative effectiveness including reproducibility issues. *Current Cardiovascular Imaging Reports*, *7*(3), 9252

77.Ma, D., Gulani, V., Seiberlich, N., Liu, K., Sunshine, J. L., Duerk, J. L., & Griswold, M. A. (2013). Magnetic resonance fingerprinting. *Nature*, *495*(7440), 187.

78.Look, D. C., & Locker, D. R. (1970). Time saving in measurement of NMR and EPR relaxation times. *Review of Scientific Instruments*, *41*(2), 250-251.

79.Gai, N., Turkbey, E. B., Nazarian, S., Van Der Geest, R. J., Liu, C. Y., Lima, J. A., & Bluemke, D. A. (2011). T1 mapping of the gadolinium-enhanced myocardium: adjustment for factors affecting interpatient comparison. *Magnetic resonance in medicine*, *65*(5), 1407-1415

80.Bieri, O., & Scheffler, K. (2006). On the origin of apparent low tissue signals in balanced SSFP. *Magnetic Resonance in Medicine: An Official Journal of the International Society for Magnetic Resonance in Medicine*, *56*(5), 1067-1074

81.Hamilton, J. I., Jiang, Y., Chen, Y., Ma, D., Lo, W. C., Griswold, M., & Seiberlich, N. (2017). MR fingerprinting for rapid quantification of myocardial T1, T2, and proton spin density. *Magnetic resonance in medicine*, *77*(4), 1446-1458

82.O h-Ici, D., Jeuthe, S., Al-Wakeel, N., Berger, F., Kuehne, T., Kozerke, S., & Messroghli, D. R. (2014). T1 mapping in ischaemic heart disease. *European Heart Journal–Cardiovascular Imaging*, *15*(6), 597-602.

83.Roy, C., Slimani, A., de Meester, C., Amzulescu, M., Pasquet, A., Vancraeynest, D., ... & Gerber, B. L. (2017). Age and sex corrected normal reference values of T1, T2 T2* and ECV in healthy subjects at 3T CMR. *Journal of Cardiovascular Magnetic Resonance*, *19*(1), 1-12)

84.Friedrich, M. G. (2010). Myocardial edema—a new clinical entity?. *Nature Reviews Cardiology*, *7*(5), 292-296)

85.Mavrogeni, S., Apostolou, D., Argyriou, P., Velitsista, S., Papa, L., Efentakis, S., ... & Manginas, A. (2017). T1 and T2 mapping in cardiology:"mapping the obscure object of desire". *Cardiology*, *138*(4), 207-217)

86.Palazón, R. P., Arqués, M. S., González, S. P., de Caralt Robira, T. M., López, M. C., & Pérez, J. O. (2015). Parametric methods for characterizing myocardial tissue by magnetic resonance imaging (part 2): T2 mapping. *Radiología (English Edition)*, *57*(6), 471-479

87.Giri, S., Chung, Y. C., Merchant, A., Mihai, G., Rajagopalan, S., Raman, S. V., & Simonetti, O. P. (2009). T2 quantification for improved detection of myocardial edema. *Journal of cardiovascular magnetic resonance*, *11*(1), 1-13

88. Von Knobelsdorff-Brenkenhoff, F., Prothmann, M., Dieringer, M. A., Wassmuth, R., Greiser, A., Schwenke, C., ... & Schulz-Menger, J. (2013). Myocardial T 1 and T 2 mapping at 3 T: reference values, influencing factors and implications. *Journal of Cardiovascular Magnetic Resonance*, *15*(1), 1-11

89.Sibley, C. T., Noureldin, R. A., Gai, N., Nacif, M. S., Liu, S., Turkbey, E. B., ... & Bluemke, D. A. (2012). T1 Mapping in cardiomyopathy at cardiac MR: comparison with endomyocardial biopsy. *Radiology*, *265*(3), 724-732.)

90.Weigel, M., Schwenk, S., Kiselev, V. G., Scheffler, K., & Hennig, J. (2010). Extended phase graphs with anisotropic diffusion. *Journal of magnetic resonance*, *205*(2), 276-285

91.Schulz-Menger, J., Bluemke, D. A., Bremerich, J., Flamm, S. D., Fogel, M. A., Friedrich, M. G., ... & Plein, S. (2013). Standardized image interpretation and post processing in cardiovascular magnetic resonance: Society for Cardiovascular Magnetic Resonance (SCMR) board of trustees task force on standardized post processing. *Journal of Cardiovascular Magnetic Resonance*, *15*(1), 35.

92.Ito, A., Yamagiwa, H., & Sasaki, R. (1980). Effects of aging on hydroxyproline in human heart muscle. *Journal of the American Geriatrics Society*, *28*(9), 398-404.

93.Liu, C. Y., Liu, Y. C., Wu, C., Armstrong, A., Volpe, G. J., Van der Geest, R. J., ... & Lima, J. A. (2013). Evaluation of age-related interstitial myocardial fibrosis with cardiac magnetic resonance contrast-enhanced T1 mapping: MESA (Multi-Ethnic Study of Atherosclerosis). *Journal of the American College of Cardiology*, *62*(14), 1280-1287

94.Van Heeswijk, R. B., Feliciano, H., Bongard, C., Bonanno, G., Coppo, S., Lauriers, N., ... & Stuber, M. (2012). Free-breathing 3 T magnetic resonance T2-mapping of the heart. *JACC: Cardiovascular Imaging*, *5*(12), 1231-1239

95.Verhaert, D., Thavendiranathan, P., Giri, S., Mihai, G., Rajagopalan, S., Simonetti, O. P., & Raman, S. V. (2011). Direct T2 quantification of myocardial edema in acute ischemic injury. *JACC. Cardiovascular imaging*, *4*(3), 269–278. https://doi.org/10.1016/j.jcmg.2010.09.023

96.Ugander, M., Bagi, P. S., Oki, A. J., Chen, B., Hsu, L. Y., Aletras, A. H., ... & Arai, A. E. (2012). Myocardial edema as detected by pre-contrast T1 and T2 CMR delineates area at risk associated with acute myocardial infarction. *JACC: Cardiovascular Imaging*, *5*(6), 596-603

97.Messroghli, D. R., Walters, K., Plein, S., Sparrow, P., Friedrich, M. G., Ridgway, J. P., & Sivananthan, M. U. (2007). Myocardial T1 mapping: application to patients with acute and chronic myocardial infarction. *Magnetic Resonance in Medicine: An Official Journal of the International Society for Magnetic Resonance in Medicine*, *58*(1), 34-40

98.Hamlin, S. A., Henry, T. S., Little, B. P., Lerakis, S., & Stillman, A. E. (2014). Mapping the future of cardiac MR imaging: case-based review of T1 and T2 mapping techniques. *Radiographics*, *34*(6), 1594-1611

99.Messroghli, D. R., Radjenovic, A., Kozerke, S., Higgins, D. M., Sivananthan, M. U., & Ridgway, J. P. (2004). Modified Look-Locker inversion recovery (MOLLI) for high-resolution T1 mapping of the heart. *Magnetic Resonance in Medicine: An Official Journal of the International Society for Magnetic Resonance in Medicine*, *52*(1), 141-146.

100.Deistung, A., Schweser, F., & Reichenbach, J. R. (2017). Overview of quantitative susceptibility mapping. *NMR in Biomedicine*, *30*(4), e3569.

101.Everett, R. J., Stirrat, C. G., Semple, S. I. R., Newby, D. E., Dweck, M. R., & Mirsadraee, S. (2016). Assessment of myocardial fibrosis with T1 mapping MRI. *Clinical Radiology*, *71*(8), 768-778

102.Reinstadler, S. J., Stiermaier, T., Liebetrau, J., Fuernau, G., Eitel, C., de Waha, S., ... & Lücke, C. (2018). Prognostic significance of remote myocardium alterations assessed by quantitative noncontrast T1 mapping in ST-segment elevation myocardial infarction. *JACC: cardiovascular imaging*, *11*(3), 411-419.

103.Kellman, P., Bandettini, W. P., Mancini, C., Hammer-Hansen, S., Hansen, M. S., & Arai, A. E. (2015). Characterization of myocardial T1-mapping bias caused by intramyocardial fat in inversion recovery and saturation recovery techniques. *Journal of Cardiovascular Magnetic Resonance*, *17*(1), 33

104.Dass, S., Suttie, J. J., Piechnik, S. K., Ferreira, V. M., Holloway, C. J., Banerjee, R., ... & Watkins, H. (2012). Myocardial tissue characterization using magnetic resonance noncontrast t1 mapping in hypertrophic and dilated cardiomyopathy. *Circulation: Cardiovascular Imaging*, *5*(6), 726-733

105.T1 mapping in differentiation of normal myocardium from diffuse disease in hypertrophic and dilated cardiomyopathy. *JACC: Cardiovascular Imaging*, *6*(4), 475-484)

106.Aus dem Siepen, F., Baumgärtner, C., Müller-Henessen, M., André, F., Messroghli, D., Ochs, M., ... & Buss, S. J. (2018). Variability of cardiovascular magnetic resonance (CMR) T1 mapping parameters in healthy volunteers during long-term follow-up. *Open heart*, *5*(1)

107.Moon, J. C., Messroghli, D. R., Kellman, P., Piechnik, S. K., Robson, M. D., Ugander, M., ... & Schulz-Menger, J. (2013). Myocardial T1 mapping and extracellular volume quantification: a Society for Cardiovascular Magnetic Resonance (SCMR) and CMR Working Group of the European Society of Cardiology consensus statement. *Journal of Cardiovascular Magnetic Resonance*, *15*(1), 92

108.Sibley, C. T., Noureldin, R. A., Gai, N., Nacif, M. S., Liu, S., Turkbey, E. B., ... & Bluemke, D. A. (2012). T1 Mapping in cardiomyopathy at cardiac MR: comparison with endomyocardial biopsy. *Radiology*, *265*(3), 724-732.)

109.Usman, A. A., Taimen, K., Wasielewski, M., McDonald, J., Shah, S., Giri, S., ... & Carr, J. C. (2012). Cardiac magnetic resonance T2 mapping in the monitoring and follow-up of acute cardiac transplant rejection: a pilot study. *Circulation: Cardiovascular Imaging*, *5*(6), 782-790

110.Cui, C., Wang, S., Lu, M., Duan, X., Wang, H., Jia, L., ... & Arai, A. E. (2018). Detection of recent myocardial infarction using native T1 mapping in a swine model: a validation study. *Scientific reports*, *8*(1), 1-10

111.Roujol, S., Weingärtner, S., Foppa, M., Chow, K., Kawaji, K., Ngo, L. H., ... & Nezafat, R. (2014). Accuracy, precision, and reproducibility of four T1 mapping sequences: a head-to-head comparison of MOLLI, ShMOLLI, SASHA, and SAPPHIRE. *Radiology*, *272*(3), 683-689

112.Dall'Armellina, E., Piechnik, S. K., Ferreira, V. M., Si, Q. L., Robson, M. D., Francis, J. M., Cuculi, F., Kharbanda, R. K., Banning, A. P., Choudhury, R. P., Karamitsos, T. D., & Neubauer, S. (2012). Cardiovascular magnetic resonance by non contrast T1-mapping allows assessment of severity of injury in acute myocardial infarction. *Journal of cardiovascular magnetic resonance : official journal of the Society for Cardiovascular Magnetic Resonance*, *14*(1), 15. https://doi.org/10.1186/1532-429X-14-15

113.Nakamori, S., Alakbarli, J., Bellm, S., Motiwala, S. R., Addae, G., Manning, W. J., & Nezafat, R. (2017). Native T1 value in the remote myocardium is independently associated with left ventricular dysfunction in patients with prior myocardial infarction. *Journal of Magnetic Resonance Imaging*, *46*(4), 1073-1081

114.Tsai, I. T., Wang, C. P., Lu, Y. C., Hung, W. C., Wu, C. C., Lu, L. F., ... & Yu, T. H. (2017). The burden of major adverse cardiac events in patients with coronary artery disease. *BMC cardiovascular disorders*, *17*(1), 1

115.Okur, A., Kantarcı, M., Kızrak, Y., Yıldız, S., Pirimoğlu, B., Karaca, L., ... & Sevimli, S. (2014). Quantitative evaluation of ischemic myocardial scar tissue by unenhanced T1 mapping using 3.0 Tesla MR scanner. *Diagnostic and Interventional Radiology*, *20*(5), 407

116. Solano, J. P., Gomes, B., & Higginson, I. J. (2006). A comparison of symptom prevalence in far advanced cancer, AIDS, heart disease, chronic obstructive pulmonary disease and renal disease. *Journal of pain and symptom management*, *31*(1), 58-69

117.Messroghli, D. R., Moon, J. C., Ferreira, V. M., Grosse-Wortmann, L., He, T., Kellman, P., ... & Friedrich, M. G. (2017). Clinical recommendations for cardiovascular magnetic resonance mapping of T1. *T2, T2 and extracellular volume: a consensus statement by the Society for Cardiovascular Magnetic Resonance (SCMR) endorsed by the European Association for Cardiovascular Imaging (EACVI) J Cardiovasc Magn Reson*, *19*, 75

118. Kranzusch, R., Aus Dem Siepen, F., Wiesemann, S., Zange, L., Jeuthe, S., da Silva, T. F., ... & Schulz-Menger, J. (2020). Z-score mapping for standardized analysis and reporting of cardiovascular magnetic

resonance modified Look-Locker inversion recovery (MOLLI) T1 data: Normal behavior and validation in patients with amyloidosis. *Journal of Cardiovascular Magnetic Resonance*, *22*(1), 1-10.

119.World Health Organization. (1995). *Physical status: The use of and interpretation of anthropometry, Report of a WHO Expert Committee*. World Health Organization.

120.Messroghli, D. R., Greiser, A., Fröhlich, M., Dietz, R., & Schulz-Menger, J. (2007). Optimization and validation of a fully-integrated pulse sequence for modified look-locker inversion-recovery (MOLLI) T1 mapping of the heart. *Journal of Magnetic Resonance Imaging: An Official Journal of the International Society for Magnetic Resonance in Medicine*, *26*(4), 1081-1086

121.Chow, K., Yang, Y., Shaw, P., Kramer, C. M., & Salerno, M. (2016). Robust free-breathing SASHA T 1 mapping with high-contrast image registration. *Journal of Cardiovascular Magnetic Resonance*, *18*(1), 1-14.

122.Hamilton, J. I., Jiang, Y., Ma, D., Mehta, B. B., Lo, W. C., Chen, Y., ... & Seiberlich, N. (2016). Cardiac MR fingerprinting for T1 and T2 mapping in four heartbeats. *Journal of Cardiovascular Magnetic Resonance*, *18*(1), W1.

123.Shaw, J. L., Yang, Q., Zhou, Z., Deng, Z., Nguyen, C., Li, D., & Christodoulou, A. G. (2019). Free-breathing, non-ECG, continuous myocardial T1 mapping with cardiovascular magnetic resonance multitasking. *Magnetic resonance in medicine*, *81*(4), 2450-2463

124.Bustin, A., Lima da Cruz, G., Jaubert, O., Lopez, K., Botnar, R. M., & Prieto, C. (2019). High-dimensionality undersampled patch-based reconstruction (HD-PROST) for accelerated multi-contrast MRI. *Magnetic resonance in medicine*, *81*(6), 3705–3719. https://doi.org/10.1002/mrm.27694

125.Tessa, C., Del Meglio, J., Salvatori, L., & Casolo, G. (2014). T1 and T2 mapping: new perspectives in cardiac magnetic resonance imaging. *Giornale italiano di cardiologia (2006)*, *15*(11), 607-615

126.Gold, R., Reichman, M., Greenberg, E., Ivanidze, J., Elias, E., Tsiouris, A. J., Comunale, J. P., Johnson, C. E., & Sanelli, P. C. (2010). Developing a new reference standard: is validation necessary?. *Academic radiology*, *17*(9), 1079–1082. https://doi.org/10.1016/j.acra.2010.05.021

127.Ferreira, V. M., & Piechnik, S. K. (2020). CMR Parametric Mapping as a Tool for Myocardial Tissue Characterization. *Korean circulation journal*, *50*(8), 658–676. https://doi.org/10.4070/kcj.2020.0157

128.Ghasemi, A., & Zahediasl, S. (2012). Normality tests for statistical analysis: a guide for non-statisticians. *International journal of endocrinology and metabolism*, *10*(2), 486–489. https://doi.org/10.5812/ijem.3505

129.McHugh M. L. (2012). Interrater reliability: the kappa statistic. *Biochemia medica*, *22*(3), 276–282

130. White, S. K., Sado, D. M., Flett, A. S., & Moon, J. C. (2012). Characterising the myocardial interstitial space: the clinical relevance of non-invasive imaging. *Heart*, *98*(10), 773-779

131. Sundjaja, J. H., Shrestha, R., & Krishan, K. (2021). McNemar And Mann-Whitney U Tests. *StatPearls [Internet]*

132.Kancharla, K., Weissman, G., Elagha, A. A., Kancherla, K., Samineni, S., Hill, P. C., ... & Fuisz, A. R. (2016). Scar quantification by cardiovascular magnetic resonance as an independent predictor of long-term survival in patients with ischemic heart failure treated by coronary artery bypass graft surgery. *Journal of Cardiovascular Magnetic Resonance*, *18*(1), 1-9

133.Messroghli, D. R., Moon, J. C., Ferreira, V. M., Grosse-Wortmann, L., He, T., Kellman, P., ... & Friedrich, M. G. (2017). Clinical recommendations for cardiovascular magnetic resonance mapping of T1, T2, T2* and extracellular volume: a consensus statement by the Society for Cardiovascular Magnetic Resonance (SCMR) endorsed by the European Association for Cardiovascular Imaging (EACVI). *Journal of Cardiovascular Magnetic Resonance*, *19*(1), 1-24

134.Christodoulou, A. G., Shaw, J. L., Nguyen, C., Xie, Y., Wang, N., Yang, Q., & Li, D. Non-ECG, free-breathing myocardial T1-T2 mapping of acute myocardial infarction using low-rank tensor MR multitasking

135.Cavallo, A. U., Liu, Y., Patterson, A., Al-Kindi, S., Hamilton, J., Gilkeson, R., ... & Rajagopalan, S. (2019). CMR fingerprinting for myocardial T1, T2, and ECV quantification in patients with nonischemic cardiomyopathy. *JACC: Cardiovascular Imaging*, *12*(8 Part 1), 1584-1585

136. Aus dem Siepen, F., Baumgärtner, C., Müller-Henessen, M., André, F., Messroghli, D., Ochs, M., Riffel, J., Giannitsis, E., Katus, H. A., Friedrich, M. G., & Buss, S. J. (2018). Variability of cardiovascular magnetic resonance (CMR) T1 mapping parameters in healthy volunteers during long-term follow-up. *Open heart*, *5*(1), e000717. https://doi.org/10.1136/openhrt-2017-000717

137.Valbuena-López, S., Hinojar, R., & Puntmann, V. O. (2016). Cardiovascular magnetic resonance in cardiology practice: a concise guide to image acquisition and clinical interpretation. *Revista Española de Cardiología (English Edition)*, *69*(2), 202-210

138. Kolentinis M, Carerj LM, Vidalakis E, Giokoglu E, Martin S, Arendt C, et al. Determination of scar area using native and post-contrast T1 mapping: Agreement with late gadolinium enhancement. European Journal of Radiology. 2022. p. 110242. doi:10.1016/j.ejrad.2022.110242

139.Haqqani, H. M., & Marchlinski, F. E. (2009). Electrophysiologic substrate underlying postinfarction ventricular tachycardia: characterization and role in catheter ablation. *Heart Rhythm*, *6*(8), S70-S76

140.Iles, L. M., Ellims, A. H., Llewellyn, H., Hare, J. L., Kaye, D. M., McLean, C. A., & Taylor, A. J. (2015). Histological validation of cardiac magnetic resonance analysis of regional and diffuse interstitial myocardial fibrosis. *European Heart Journal-Cardiovascular Imaging*, *16*(1), 14-22.

141.Ferreira, V. M., Piechnik, S. K., Dall'Armellina, E., Karamitsos, T. D., Francis, J. M., Choudhury, R. P., ... & Neubauer, S. (2012). Non-contrast T1-mapping detects acute myocardial edema with high diagnostic accuracy: a comparison to T2-weighted cardiovascular magnetic resonance. *Journal of cardiovascular magnetic resonance*, *14*(1), 1-12

142.Ugander, M., Bagi, P. S., Oki, A. J., Chen, B., Hsu, L. Y., Aletras, A. H., Shah, S., Greiser, A., Kellman, P., & Arai, A. E. (2012). Myocardial edema as detected by pre-contrast T1 and T2 CMR delineates area at risk associated with acute myocardial infarction. *JACC. Cardiovascular imaging*, *5*(6), 596–603. https://doi.org/10.1016/j.jcmg.2012.01.016

143.Leiner, T., Rueckert, D., Suinesiaputra, A., Baeßler, B., Nezafat, R., Išgum, I., & Young, A. A. (2019). Machine learning in cardiovascular magnetic resonance: basic concepts and applications. *Journal of Cardiovascular Magnetic Resonance*, *21*(1), 1-14.

144.Beek, A. M., Nijveldt, R., & van Rossum, A. C. (2010). Intramyocardial hemorrhage and microvascular obstruction after primary percutaneous coronary intervention. *The international journal of cardiovascular imaging*, *26*(1), 49-55

145. Ganame, J., Messalli, G., Dymarkowski, S., Rademakers, F. E., Desmet, W., Van de Werf, F., & Bogaert, J. (2009). Impact of myocardial haemorrhage on left ventricular function and remodelling in patients with reperfused acute myocardial infarction. *European heart journal*, *30*(12), 1440-1449

146.Fox, C. S., Muntner, P., Chen, A. Y., Alexander, K. P., Roe, M. T., Cannon, C. P., ... & Wiviott, S. D. (2010). Use of evidence-based therapies in short-term outcomes of ST-segment elevation myocardial infarction and non-ST-segment elevation myocardial infarction in patients with chronic kidney disease: a report from the National Cardiovascular Data Acute Coronary Treatment and Intervention Outcomes Network registry. *Circulation*, *121*(3), 357-365)

147.Weinreb, J. C., Rodby, R. A., Yee, J., Wang, C. L., Fine, D., McDonald, R. J., ... & Davenport, M. S. (2020). Use of Intravenous Gadolinium-based Contrast Media in Patients with Kidney Disease: Consensus Statements from the American College of Radiology and the National Kidney Foundation. *Kidney Medicine*

148. Ferreira, V. M., & Piechnik, S. K. (2020). CMR Parametric Mapping as a Tool for Myocardial Tissue Characterization. *Korean circulation journal*, *50*(8), 658–676. https://doi.org/10.4070/kcj.2020.0157

149.Kloner, R. A. (2020). Stunned and hibernating myocardium: where are we nearly 4 decades later?. *Journal of the American Heart Association*, *9*(3), e015502

150. Baer, F. M., Voth, E., Schneider, C. A., Theissen, P., Schicha, H., & Sechtem, U. (1995). Comparison of low-dose dobutamine–gradient-echo magnetic resonance imaging and positron emission tomography with [18F] fluorodeoxyglucose in patients with chronic coronary artery disease: a functional and morphological approach to the detection of residual myocardial viability. *Circulation*, *91*(4), 1006-1015.

151.Walker, Esteban, and Amy S Nowacki. "Understanding equivalence and noninferiority testing." *Journal of general internal medicine* vol. 26,2 (2011): 192-6. doi:10.1007/s11606-010-1513-8

152.Kali, A., Cokic, I., Tang, R. L., Yang, H. J., Sharif, B., Marbán, E., ... & Dharmakumar, R. (2014). Determination of location, size, and transmurality of chronic myocardial infarction without exogenous contrast media by using cardiac magnetic resonance imaging at 3 T. *Circulation: Cardiovascular Imaging*, *7*(3), 471-481

153. Friedrich MG, Abdel-Aty H, Taylor A, Schulz-Menger J, Messroghli D, Dietz R. The salvaged area at risk in reperfused acute myocardial infarction as visualized by cardiovascular magnetic resonance. J Am Coll Cardiol. 2008;51: 1581–1587.

154. https://www.lexico.com/definition/ground-truth

155. Stock, E. O., & Redberg, R. (2012). Cardiovascular disease in women. *Current problems in cardiology*, *37*(11), 450-526

156. Doody, M. M., Freedman, D. M., Alexander, B. H., Hauptmann, M., Miller, J. S., Rao, R. S., ... & Linet, M. S. (2006). Breast cancer incidence in US radiologic technologists. *Cancer: Interdisciplinary International Journal of the American Cancer Society*, *106*(12), 2707-2715

157. Ordovas, K. G., Baldassarre, L. A., Bucciarelli-Ducci, C., Carr, J., Fernandes, J. L., Ferreira, V. M., ... & Srichai, M. B. (2021). Cardiovascular magnetic resonance in women with cardiovascular disease: position statement from the Society for Cardiovascular Magnetic Resonance (SCMR). *Journal of Cardiovascular Magnetic Resonance*, *23*(1), 1-17

Image references:

1.https://www.medicinenet.com/heart_attack/article.htm

2.Sprawls, P. (1993). *Physical principles of medical imaging*. Gaithersburg: Aspen Publishers. Chapter 3.

3. Ridgway, J. P. (2010). Cardiovascular magnetic resonance physics for clinicians: part I. *Journal of cardiovascular magnetic resonance*, *12*(1), 1-28

4. Bitar, R., Leung, G., Perng, R., Tadros, S., Moody, A. R., Sarrazin, J., ... & Roberts, T. P. (2006). MR pulse sequences: what every radiologist wants to know but is afraid to ask. *Radiographics*, *26*(2), 513-537.

5. Higgins, C.B.;de ROOS, Albert. Cardiovascular MRI AND mra. LWW. 2002

6. Gräni, C., Eichhorn, C., Bière, L., Kaneko, K., Murthy, V. L., Agarwal, V., ... & Kwong, R. Y. (2019). Comparison of myocardial fibrosis quantification methods by cardiovascular magnetic resonance imaging for risk stratification of patients with suspected myocarditis. *Journal of Cardiovascular Magnetic Resonance*, *21*(1), 1-11

7. Karamitsos, T. D., Francis, J. M., Myerson, S., Selvanayagam, J. B., & Neubauer, S. (2009). The role of cardiovascular magnetic resonance imaging in heart failure. *Journal of the American College of Cardiology*, *54*(15), 1407-1424

8. https://www.crit.cloud/world-of-foam/category/sonography

9. Magrath, P., Maforo, N., Renella, P., Nelson, S. F., Halnon, N., & Ennis, D. B. (2018). Cardiac MRI biomarkers for Duchenne muscular dystrophy. *Biomarkers in medicine*, *12*(11), 1271-1289.

10. Messroghli, D. R., Moon, J. C., Ferreira, V. M., Grosse-Wortmann, L., He, T., Kellman, P., ... & Friedrich, M. G. (2017). Clinical recommendations for cardiovascular magnetic resonance mapping of T1, T1, T2* and extracellular volume: a consensus statement by the Society for Cardiovascular Magnetic Resonance (SCMR) endorsed by the European Association for Cardiovascular Imaging (EACVI). *Journal of Cardiovascular Magnetic Resonance*, *19*(1), 1-24.

11. Taylor, R. J., Moody, W. E., Umar, F., Edwards, N. C., Taylor, T. J., Stegemann, B., ... & Leyva, F. (2015). Myocardial strain measurement with feature-tracking cardiovascular magnetic resonance: normal values. *European Heart Journal–Cardiovascular Imaging*, *16*(8), 871-881.

12. Tran, T. T., Tran, T. T., Ninh, Q. C., Bui, M. D., & Pham, V. T. (2020, November). Segmentation of Left Ventricle in Short-Axis MR Images Based on Fully Convolutional Network and Active Contour Model. In *International Conference on Green Technology and Sustainable Development* (pp. 49-59). Springer, Cham.